

<https://doi.org/10.1590/2318-0331.292420230139>

Dramatic changes in the confluence morphology driven by an extreme hydrologic pulse: impacts to River Doce restoration

Mudanças intensas na morfologia da confluência impulsionadas por um pulso hidrológico extremo: impactos na restauração do Rio Doce

Alexandre Germano Marciano¹ , Arcilan Trevenzoli Assireu¹ , Samara Calçado de Azevedo¹ , Benedito Cláudio da Silva¹ ,
Adriana Tropia de Abreu²  & Hermínio Arias Nalini Júnior² 

¹Universidade Federal de Itajubá, Itajubá, MG, Brasil

²Universidade Federal de Ouro Preto, Ouro Preto, MG, Brasil

E-mails: agermano@unifei.edu.br (AGM), arcilan@unifei.edu.br (ATA), samara_calcado@unifei.edu.br (SCA), silvabenedito@unifei.edu.br (BCS),
adriana.abreu@ufop.edu.br (ATA), nalini@ufop.edu.br (HANJ)

Received: December 01, 2023 - Revised: January 25, 2024 - Accepted: February 05, 2024

ABSTRACT

On January 2022, the Carmo River (a tributary of the Doce River) was affected by an extreme hydrological event, with 50-yr return interval. This event was 50% higher than that associated to one of the largest tailing dam failures ever reported that took place in the Gualaxo do Norte River. This delivered to Doce River, through the Carmo River, in a Y-shaped confluence, the contaminated tailing slurry. In order to understand the role of tributaries in the recovery of the Doce River, 2D hydrodynamic and 2D sediment transport models were applied at the confluence of the Carmo River with the Piranga River. Our results, based on hydraulic modeling, remote sensing, and in-situ measurements, indicated that significant amounts of sediments were trapped on the riverbanks and stone banks, making this confluence an important site for the retention of contaminated sediments, influencing sediment budgets and downstream water quality. Therefore, this confluence deserves special attention from water engineering in order to prevent the sediments retained in this area from being transported downstream during extreme events in the coming years. These results can contribute to decision-making, to identify reaches with greater susceptibility to erosion and sediment deposition and to plan the restoration of these rivers.

Keywords: River confluence; Hydraulic modeling; River restoration; Sediment transport; Morphodynamics.

RESUMO

Em janeiro de 2022, o Rio Carmo (um afluente do Rio Doce) foi afetado por um evento hidrológico extremo, com um tempo de retorno de 50 anos. Esse evento foi 50% mais intenso do que o associado a uma das maiores falhas de barragem de rejeitos já registradas, que ocorreu neste mesmo rio. Isso resultou no despejo de rejeitos de mineração contaminados no Rio Doce, por meio do Rio Carmo, em uma confluência em forma de Y. Com objetivo de entender a função dos afluentes na recuperação do rio Doce, foram realizadas simulações hidrodinâmicas e de transporte de sedimentos, a partir da versão bidimensional do modelo HEC-RAS, na confluência do rio do Carmo com o rio Piranga. Nossos resultados, com base em modelagem numérica, sensoriamento remoto e medições in situ, apontaram que grandes quantidades de sedimentos foram retidas nas margens do rio e nos bancos de pedra, o que torna esta confluência um local importante para a retenção de sedimentos contaminados, com influências significativas para a qualidade de água a jusante. Sendo assim, essa confluência merece uma atenção especial da engenharia Hídrica a fim de evitar que os sedimentos retidos nesta área sejam transportados a jusante durante os eventos extremos nos próximos anos. Esses resultados podem contribuir para a tomada de decisões, para identificação de trechos com maior suscetibilidade a erosão e deposição de sedimento e para planejamento da restauração desses rios.

Palavras-chave: Confluência de rios; Modelagem hidráulica; Restauração de rios; Transporte de sedimentos; Morfodinâmica.



INTRODUCTION

River confluences are where rivers meet and are therefore fundamental components of natural channel drainage networks (Shukla et al., 2022a). The river confluence is an environment with continuous changes in the flow structure such as speed, direction and flow rate (Best & Rhoads, 2008; Yuan et al., 2022); in the composition of sediments and nutrients (Nazari-Giglou et al., 2016; Yu et al., 2020); and in the morphology of the receptor channel (Best & Roy, 1991; Sukhodolov et al., 2023).

Abrupt changes in the hydraulic characteristics of rivers generally occur at confluences (Rhoads, 2020) because of the interactions of hydraulic variables. Furthermore, confluences are of great importance in the river ecosystem, as they enable the occurrence of biophysical and ecosystem processes from the interaction of two often distinct basins (Rice et al., 2008; Samson, et al., 2019).

The geomorphological processes that occur at confluences have attracted scientific interest in recent decades. These interests derive from the understanding that river processes summarize the physical characteristics of the upstream watershed. Furthermore, they also generate information about hydrodynamics and sediments in the downstream drainage network (Santos & Stevaux, 2017; Luz et al., 2020).

Best (1987) and Liu et al. (2019) defined the flow behavior of confluences in six flow zones: stagnation zone (where deflection of both flows occurs at the junction); deflection zone (where flow recirculation occurs); separation zone (where the change in flow direction occurs); zone of maximum speed (junction of flows after the separation zone); restoration zone (where the flow gradually recovers) and shear layers (areas stagnant with the flow). Rhoads & Kenworthy (1995) defined these zones as the Confluence Hydrodynamic Zone (CHZ).

Best & Rhoads (2008) and Bilal et al. (2020) identified five main morphological characteristics that may be present or absent in a confluence: excavation zone (characterized by a depression in the receiving channel caused by bed erosion); tributary bar (accumulation of sediment at the mouth of one or both channels); central bar (sediment accumulation after the excavation zone); side bar (accumulation of sediment on the sides); and, region of sediment accumulation (located at the corner of the junction, upstream).

Some human interventions alter the morphological characteristics of confluences, such as: the extraction of sediments from the riverbed (Calle et al., 2017; Dawson, 2021), channelization (Zawiejska et al., 2015; Laurence et al., 2022), the construction of dams (Sanchis-Ibor et al., 2018; Thomson et al., 2022), and changes in land use and land cover (Fortugno et al., 2017; Magliulo et al., 2021). In particular, in this work, we will be investigating how the hydrological pulse interferes in a confluence impacted by one of the biggest environmental disasters known, the Mariana disaster – MG.

Another factor that can modify morphological characteristics is climate change (Cienciala & Pasternack, 2017; Anim-Gyampo et al., 2019), especially extreme floods that can produce notable changes in the channel in a very short period, often with long-lasting geomorphological effects. (Righini et al., 2017; Magliulo & Valente, 2020).

One of the ways to reproduce/show changes in the morphology of confluences is through numerical models (1D, 2D and 3D). Some models simulate flow and sediment transport, using hydraulic variables and sediment properties (Yan et al., 2022), which allow: calculating sediment deposition and erosion; evaluate the sediment balance and; identify critical points and areas prone to deposition or erosion (Edmonds et al., 2023).

The HEC-RAS (Hydrologic Engineering Center - River Analysis System) program has been widely used, around the world, in research related to modeling sediment transport in river channels. Since its creation in 1995 and its last update in August 2022, the model has demonstrated consistent performance and is compatible with field measurements, demonstrating its potential to contribute to studies on hydrosedimentation. The review by Das & Senthil Vadivel (2022) highlights the continued effectiveness of HEC-RAS, with positive results being observed since 2003. Examples of studies that have used HEC-RAS to model sediment transport include research such as: Duan et al. (2008) evaluated the model for the Rillito River in Arizona, USA; Haghiabi & Zaredehdasht (2012) investigated sedimentation prediction in the Karun River, Iran; Azarang & Bajestan. (2015) simulated the sedimentation process in river and floodplain areas in a river basin in northern Germany; Berghout, & Meddi (2016) conducted a sediment transport modeling study in the Wadi River, Chemora, Algeria; Mohammed et al. (2018) investigated the sedimentation pattern in a section of the Euphrates River in Iraq and; Shelley (2021) simulated sediment transport to predict deposition in the Missouri River, USA. More recently, Damte et al. (2021) used HEC-RAS to estimate sedimentation activities to predict floods in the Kulfo River, in Ethiopia and; Ghosh et al. (2021) evaluated the lateral erosion of the banks of the Bhagirathi-Hooghly River, in India. Corum et al. (2023), Gudgeirdóttir (2023) and Marx (2023) employed the HEC-RAS (6.3) program to model two-dimensional sediment transport. These studies collectively demonstrate the continued relevance and effectiveness of HEC-RAS as a modeling tool for hydrodynamic and sediment transport analyzes in river environments. The application of this model for hydrosedimentological studies in Brazil, to the best of our knowledge, is being carried out in this work.

The Doce river basin is a basin impacted by the tragedy that occurred on November 5, 2015, when the mining tailings dam in Mariana – MG collapsed, causing a gigantic environmental disaster that, to this day, has serious consequences for the lives of thousands of people (Lopes et al., 2019; Fraga et al., 2020; Frachini et al., 2021; Paulelli et al., 2022; Mourão et al., 2023). These sediments contain the presence of heavy metals (mercury, lead, cadmium, manganese, nickel, iron, tin, chromium and arsenic) (Frachini et al., 2021; Kroukamp & Wepener 2022).

In January 2022, a flood event occurred, which was the largest in the last 25 years and the third largest recorded in the Doce River basin (Santos et al., 2021). This caused major disruption and around 20 thousand people were left homeless (Oliveira et al., 2022). It is assumed that this event may have disturbed and transported the sediments that were accumulated at the bottom of the river channel.

This article is a contribution to the Project “Satellite-Tracked Drifters and Automatic Monitoring of Environmental Parameters Applied to Understanding the Contribution of Tributaries to the Reestablishment of the Doce River”, which consists of a

multi-instrumental and multi-institutional effort to study the influence of hydrodynamics in the region of confluences for the reestablishment of the Doce River.

In this context, this study seeks to investigate the morphological changes that occurred in response to the 2015 disaster that occurred in the Rio Doce, at a Y-shaped confluence that conceptually represents the beginning of the Rio Doce. It was also investigated whether a hydrological pulse related to intense floods that occurred in January 2022, whose intensity was the highest in the last 25 years, contributed to highlighting or minimizing the impacts resulting from the disaster. This 2022 event resulted in flow 53% greater than that observed during the disaster, presenting the potential to carry, from the bank to the river, the contaminated sediment.

STUDY AREA

The study covers the confluence of the Piranga River with the Carmo River, which is located in the Iron Quadrangle. The iron quadrangle is a region in the center-south of the state of Minas Gerais, which has the largest production of raw iron in Brazil. This confluence is formed by two river basins, the Piranga river basin, which has a drainage area of 6,612 km², and the Carmo river basin, which has a drainage area of 2,279 km². Its main tributary is the Gualaxo do Norte River, which was the river that transported iron ore tailings from the Mariana disaster to the Doce River, which occurred in November 2015, when the iron ore tailings dam collapsed. After this confluence, the watercourse is named Doce River (Sposito, 2021).

Figure 1 shows the study area where there is a confluence of the Piranga River with the Carmo River, which is classified by the geometry of the junction as symmetrical. In this type of confluence, rivers are of similar size that meet and join together

to form a single watercourse. The characteristic of this junction is that there is an acute or right angle, resulting in a symmetrical flow pattern. The junction point is shaped like a “Y” or a triangle. The combined flow of the rivers continues from this point of confluence to form the resulting downstream watercourse called the Rio Doce (Grzegorzczuk et al., 2019).

METHODOLOGY

Data sources

Data from monitoring stations

After the Mariana disaster, much attention was paid to monitoring the quality and quantity of water in the Doce River. The monitoring stations that already existed before the tragedy were updated, and new stations were created to monitor, over time, the recovery of the Doce river basin. An example is the Systematic Quali-quantitative Water and Sediment Monitoring Program (PMQQS), implemented on July 31, 2017, whose data is made available free of charge on the website (Fundação Renova, 2023).

In this study, hydrological, sedimentological and water quality data available in the National Hydrometeorological Network (RHN) of the National Water Agency (ANA) and PMQQS were used.

Initially, stations within the study area were selected, followed by a data consistency test (Estigoni, 2016), looking for possible errors (inconsistencies or failures). Data containing more than 5% error was disregarded. The ratified data were organized by date and time, in spreadsheet format, to generate graphs. After these procedures, hydrographs were created representing the flood event that occurred in January 2022.

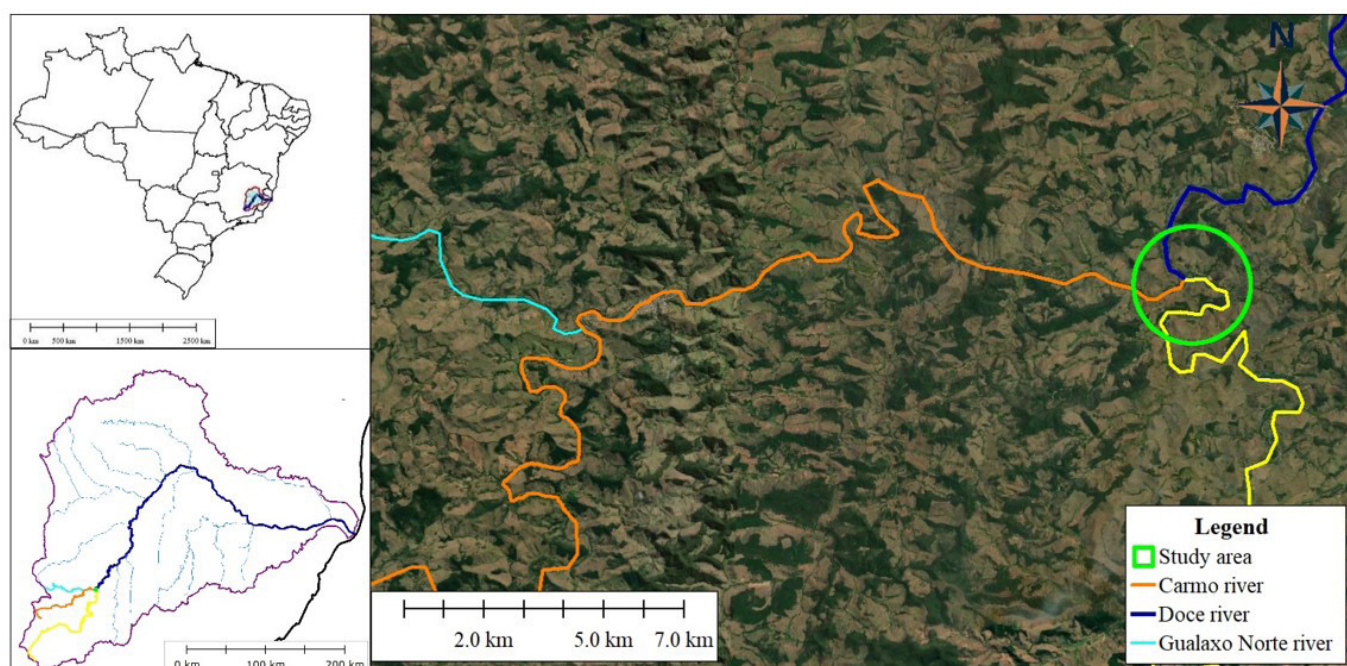


Figure 1. Location of the confluence of the Carmo River with the Piranga River. **Source:** Instituto Brasileiro de Geografia e Estatística (2016).

The stations that are upstream of the confluences served as input data to generate the model, while the stations that are downstream served to calibrate the model. Table 1 and Figure 2 present the coordinates and location of the monitoring stations used.

Using data from the stations, the return time (TR) was calculated, which is the average time in which a given natural event is equaled or surpassed (Jesus & Nascimento, 2020). To calculate return times, the probabilistic method of empirical distribution was used, according to Hallinan Junior (1993), which consists of the arrangement of the annual maximum daily flows, represented by Equations 1 and 2.

$$P = \frac{m}{n+1} \tag{1}$$

$$TR = \frac{1}{P} \tag{2}$$

where: P is the probability; m is the order of numbers; n is the amount of data in the historical series; and TR is the payback time in years.

Topographic data

Topographic data were obtained by field data collection, the ANA metadata catalog and the Digital Elevation Model (DEM) of the ALOS PALSAR - 2 satellite sensor. Details on interpolation procedure will be presented later.

During data collection in the field, planialtimetric surveys of the sections were carried out, measurements of the physical parameters of the water, flow measurements and collection of sediments on the banks and bottom of the rivers. Data collection in the field took place on September 1, 2021, the end of the dry period, to characterize the banks and to avoid contamination of the water that runs off from the rain.

The equipment used was: GNSS receivers model Leica CS09, L1/, L2, for collecting topographic points and georeferencing; Hanna multiparameter probe model HI9828, for measuring the physical and chemical parameters of water; Qliner V3 flow meter, for surveying topobathymetric sections and flows and; Van Veen type samplers for collecting sediment from the banks and bottom. Figure 3 shows some equipment used in field data collection.

The ANA metadata catalog is a source of varied data from the National Water Resources Information System (SNIRH). This database has geographic, hydrological and hydraulic

information on Brazilian hydrography. In this study, data from topobathymetric sections of the Doce river basin were used. These data were collected, processed and presented by a private company hired by a consortium of companies (CBG-DOCE, IBIO Doce and ANA), to provide topography and bathymetry services, which are available free of charge on the ANA catalog website (Brasil, 2023).

Another source of data used was from the ALOS satellite (Advanced Land Observing Satellite), which was launched on January 24, 2006 by the Japan Aerospace Exploration Agency (JAXA), at the Tanegashima space center (Japan) and entered the operational phase of data provision. to the public on October 24, 2006. One of the radars attached to the satellite is PALSAR (Phased Array L-band Synthetic Aperture Radar), which is a synthetic aperture radar that operates in the L Band, capable of obtaining day or night images and in any atmospheric conditions. The Alaska Satellite Facility project processed these images, making a radiometric correction of the terrain, generating a product of altimetric images with a spatial resolution of 12.5 m, in the GEO TIFF (Georeferenced Tagged Image File) format, made available free of charge on the website (Alaska Satellite Facility, 2023).

With these three data sources, the DEM for the study area was created. The DEM of the study area was carried out using a GIS (Geographic Information System) program. To create the DEM, the watercourse channels were created, through interpolation of topobathymetric sections, using data collected in fields and data from the ANA metadata catalog. Data from the ALOS PALSAR-2 satellite was to complement the gaps in the DEM.

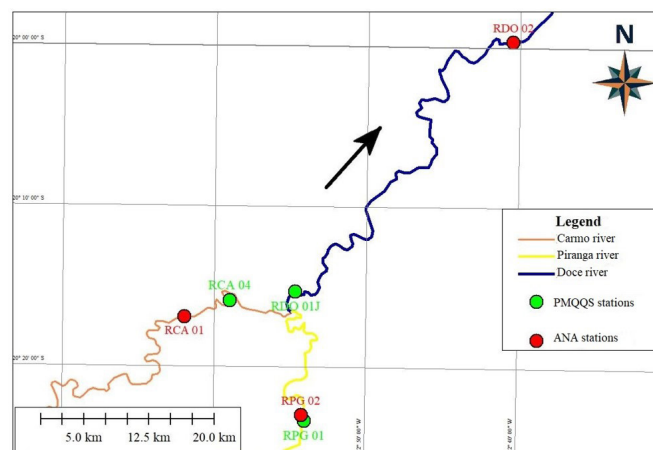


Figure 2. Location of stations in the study area.

Table 1. Location of stations.

Stations	Latitude	Longitude	Data Matrix
RCA 01 – Carmo River	20° 16' 58.08" S	43° 01' 55.92" W	Liquid discharge
RPG 02 – Piranga River	20° 23' 02.04" S	42° 54' 10.08" W	Liquid discharge
RDO 02 – Doce River	19° 59' 39.84" S	42° 40' 27.84" W	Liquid discharge
RCA 04 - Carmo River	20° 15' 54.51" S	42° 58' 56.90" W	Sediment
RPG 01 – Piranga River	20° 23' 22.55" S	42° 53' 57.46" W	Sediment
RDO 01J – Doce River	20° 15' 20.23" S	42° 54' 38.16" W	Sediment

Image data

The images were obtained from surveys carried out by a remotely piloted aircraft (ARP) equipped with a photogrammetric camera. After the survey, the reconstruction and map-making process were carried out. These images were collected, processed and presented as orthophotos with a GSD (Ground Sample Distance) of 10 cm by a private company hired by the Renova Foundation. The Renova Foundation is the entity responsible for mobilizing to repair the damage caused by the collapse of the Fundão dam, in Mariana (MG).

The Renova Foundation made available 3 orthophotos of the study area, showing the before, during and after the flood event that occurred in January 2022 (Figure 4). Table 2 presents details from the acquisition period of orthophotos.

Table 2. Orthophoto acquisition period.

Orthophotos	Period
Orthophoto (before the event)	April to May 2021
Orthophoto (during the event)	January to March 2022
Orthophoto (after the event)	June to July 2022



Figure 3. Equipment used in fieldwork: (A) Van Veen type sampler; (B) Hanna HI9828 multiparameter probe; (C) Qliner V3 and flow meter; (D) Leica LI and L2 GNSS receiver.

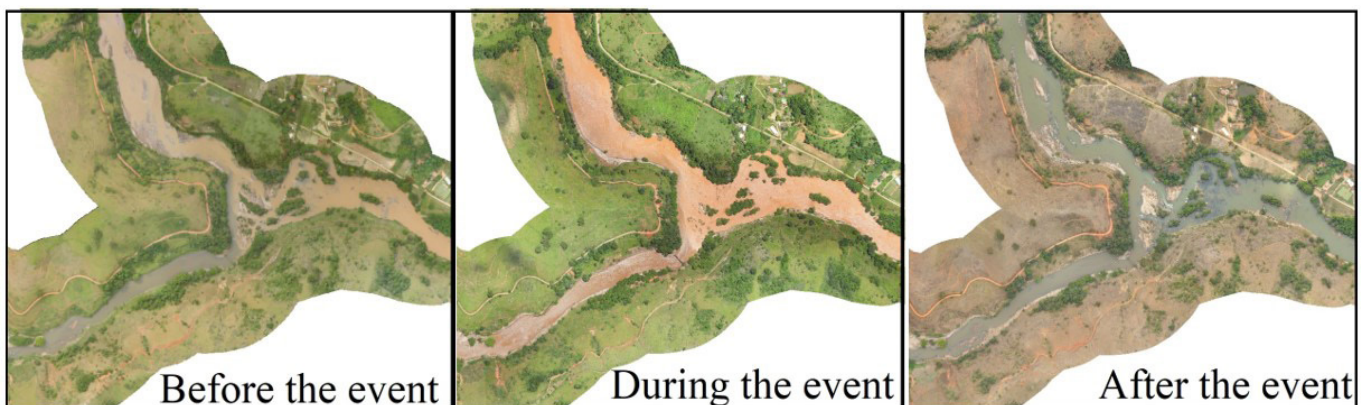


Figure 4. Orthophotos of the study area, showing the before, during and after the flooding event that occurred in January 2022.

The orthophotos were used to evaluate the hydrodynamic and sediment transport models. In the first, the area of the flood spot was statistically evaluated. In the second, the sedimentation and erosion zones indicated by the simulation were evaluated.

Models

2D hydrodynamic modeling

To solve the 2D hydrodynamic model, the HEC-RAS version 6.4.1 program was used, which solves the mass and momentum conservation equations using an implicit finite difference scheme developed by Holly Junior & Preissmann (1977) and Chen & Falconer (1992).

The two-dimensional equations were obtained from the one-dimensional equations, integrating the vertical between the bottom and the surface, considering the Cartesian x and y directions. Equations 3, 4 and 5 are the solutions of the mass and momentum conservation equations, in a plane parallel to the bottom of the channel that the HEC-RAS program solves. (Andrade, 2020).

$$\frac{\partial h}{\partial t} + u \frac{\partial u}{\partial x} + v \frac{\partial v}{\partial y} = 0 \quad (3)$$

$$\frac{\partial u}{\partial t} + u \frac{\partial u}{\partial x} + v \frac{\partial u}{\partial y} = -gh \frac{\partial H}{\partial x} - \frac{gn^2}{7} |u|u + 2\omega \sin \varphi h v + A_t \nabla^2 h u \quad (4)$$

$$\frac{\partial v}{\partial t} + u \frac{\partial v}{\partial x} + v \frac{\partial v}{\partial y} = -gh \frac{\partial H}{\partial y} - \frac{gn^2}{7} |v|v + 2\omega \sin \varphi h u + A_t \nabla^2 h v \quad (5)$$

where: h is the depth; u, v are the average speeds in the directions of x and y ; H is the elevation of the water; ω is the angular velocity of the earth; φ is the latitude and; A_t is the turbulent viscosity coefficient.

The input data are the previously worked data, which were inserted by the geometric data editor of the HEC-RAS program to create the strands measuring 5 m x 5 m in the main gutter and 10 m x 10 m in the secondary gutter. The Manning roughness values for the main and secondary gutters were calculated according to the proposal by Chow (1959) where n is determined by the physical characterization of the channel and m is the degree of sinuosity, according to Equation 6.

$$n = (n_0 + n_1 + n_2 + n_3 + n_4) \cdot m_s \quad (6)$$

The hydrographs obtained from the monitoring stations were inserted into the HEC-RAS program considering the period from 01/01/2022 to 03/30/2022. During this period, one of the largest flood events ever recorded in the region occurred.

The model was calibrated using the HEC-RAS program, adjusting the Manning coefficient for all sections, between 0.030 and 0.070, to find the best fit between the simulated hydrograph and that of the downstream monitoring station.

To adjust the calibration, Equations 7, 8 and 9 were used, which express the comparison between the hydrographs and

the determination of the coefficient (r^2). Equation 6 calculates the proportion of variation in observed values compared to the simulated variable (Rangel, 2021).

$$SSE = \sum (y - \hat{y})^2 \quad (7)$$

$$SST = \sum (y - \bar{y})^2 \quad (8)$$

$$r^2 = 1 - \frac{SSE}{SST} \quad (9)$$

where: SSE is the quadratic sum of the error; SST is the total sum of squares; y is the observed value; \bar{y} is the average of the observed values; and \hat{y} is the calculated/simulated value.

2D sediment transport modeling

To solve the 2D sediment transport model, the HEC-RAS version 6.4.1 program was used, which solves Equation 10 of bed material load transport, separating the bed material load into bed load and suspended loads with empirical formulas. Equation 7 is solved with an implicit finite volume scheme on the same mesh as the hydrodynamic model (Nelson et al., 2023).

$$\frac{\partial}{\partial t} \left(\frac{h C_{t k}}{\beta_{t k}} \right) + \nabla \cdot (h U C_{t k}) = \nabla \cdot (\epsilon_{t k} h \nabla C_{t k}) + E_{t k}^{HF} - D_{t k}^{HF} + S_{t k} \quad (10)$$

where: $C_{t k}$ is the total sediment concentration load; $\beta_{t k}$ is the total load correction factor for the particle size class; U is the average speed at depth; h is the depth of the water; $\epsilon_{t k}$ is the total charge diffusion (mixing) coefficient; $E_{t k}^{HF}$ is the total load erosion rate; $D_{t k}^{HF}$ is the total charge deposition rate and; $S_{t k}$ is the total load source/sink term.

$\epsilon_{t k}$ is the total load horizontal mixing/diffusion coefficient, determined by Equation 11.

$$\epsilon_{t k} = r_{s k} \epsilon_{s k} + (1 - r_{s k}) \epsilon_{b k} \quad \text{para } k = 1, \dots, N \quad (11)$$

where: $r_{s k}$ is the fraction of suspended load; $\epsilon_{s k}$ is the suspended load mixing coefficient; $\epsilon_{b k}$ is the bed load mixing coefficient.

The horizontal mixing coefficient of suspended load ($\epsilon_{s k}$) represents the effects of turbulent diffusion. Assuming that the horizontal sediment mixing coefficient is related to the eddy viscosity. The horizontal diffusion coefficient of the bedload ($\epsilon_{b k}$) represents the mixing of sediments due to spatially and temporally varying bedload velocities.

The input data is the data already worked on previously. Sediment data were entered into the sediment data editor of the HEC-RAS program.

The sediment transport equation applied in the model was that of Wu (2004) due to the depth of the rivers. The grain classification equation was chosen from Copeland & Thomas (1989) due to the extensive ability to calculate grain size. The fall speed equation chosen was from Wu & Wang (2006), which takes into account the shape of the particle. The granulometry was inserted for each water course according to the data collected by the field survey and data obtained from monitoring stations. The boundary condition used was the equilibrium load boundary, as the other modes require additional data, which were not collected.

Calibration of the sediment transport simulation was done in the HEC-RAS program, adjusting the transport function. The transport function controls the rate of erosion and deposition. This parameter is responsible for temporal delays in deposition and erosion. Longer fitting lengths will slow erosion and deposition, smoothing the result. Shorter lengths increase erosion and deposition. The amount recommended by the program is 10 m for rivers measuring 30 to 100 m.

RESULTS AND DISCUSSIONS

The results are presented in 3 stages. The first stage consists of creating the hydrographs that were inserted into the HEC-RAS program and creating the digital terrain model. The second stage presents the results of 2D hydrodynamic and 2D sediment transport simulations. The third stage is the evaluation of the models.

Data sources

Data from monitoring stations

To generate the hydrographs of the monitoring stations, consistency tests were carried out on the data, for greater reliability in the simulation. The procedures were carried out following the studies by Alves (2017) and Rosa (2017). Spreadsheets were then created with the hydrographs of the stations, according to a study by Marciano (2019). Figures 5, 6 and 7 show the hydrographs with the historical series (50 years of data) and with the 5-year, 10-year and 50-year TRs.

Figure 5 shows the records from station RCA 01. The biggest floods occurred in the years 1979, 1997 and 2022 (Batista, 2022; Campana, 2022; Coelho Filho et al., 2022), these have a TR greater than 50 years. The biggest flood occurred on February 3, 1979 with a flow of 733 m³/s. For comparison purposes, for the anthropogenic Mariana – MG disaster, there was a flow of 414 m³/s, equivalent to a TR of 10 years. In the January 2022 event, the flow reached 637 m³/s on January 11, being the highest in the last 25 years and 53% greater than that of the Mariana – MG disaster. Since the Rio do Carmo was the river that carried the mud from the Mariana disaster to the Rio Doce, the occurrence of a flood pulse with an intensity so much greater than that of the accident itself, anticipates the possibility that natural events could contribute for the remobilization of sediments deposited on the bank.

Figure 6 shows the records from station RPG 02. The biggest floods occurred in 1997 and 2012, with a TR of more than 50 years. The biggest flood occurred on January 4, 2012 with a flow of 1312 m³/s. The event reached a flow of 849 m³/s, on January 11, 2022, being the fourth highest flow recorded, with a TR of 13 years. The Mariana – MG disaster was not recorded at this station, as it is upstream of the confluence. The flow of the Piranga River is, on average, 3 times that of the Carmo River, anticipating the importance of this river for the recovery of the Doce River.

Figure 7 shows the records from station RDO 02. The biggest floods occurred in the years 1997 and 2022, with a TR

greater than 50 years. The biggest flood occurred on January 5, 1997 with a flow of 2236 m³/s. In the Mariana disaster – MG there was a flow of 871 m³/s equivalent to a TR of 3 years. In the January 2022 event, a flow rate of 2000 m³/s was reached on February 10, 2022, the highest in the last 25 years. Note that the peak flow, in this case, is one month behind what was observed in the two previous cases. This is due to the fact that this station is downstream of the Risoleta Neves UHE, which played a role in regulating the flow.

Data from stations RCA 01 and RPG 02 were used as input data in the HEC-RAS program. The RDO 02 station was used to calibrate the model.

The granulometric curve of the sediments was made using data from monitoring stations and field data surveys. Figure 8 shows the particle size distribution, collected in September 2021. The Doce River has a greater amount of coarse particles (sand) than the Carmo River and the Piranga River. The Carmo River, 36% fine sand and 34% medium sand. The Piranga River has 36% fine sand particles and 24% medium sand.

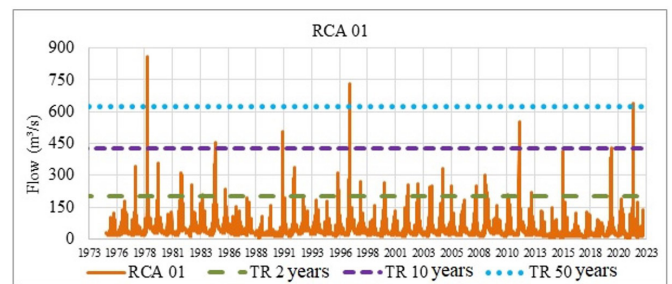


Figure 5. Carmo River Station.

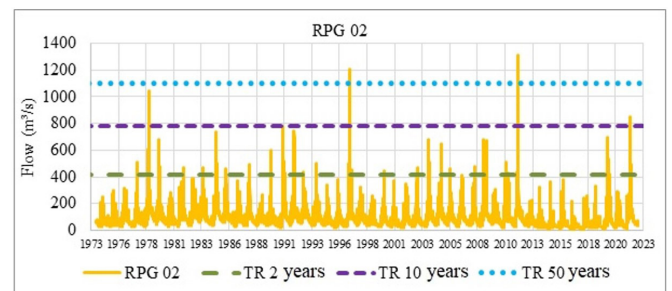


Figure 6. Piranga River Station.

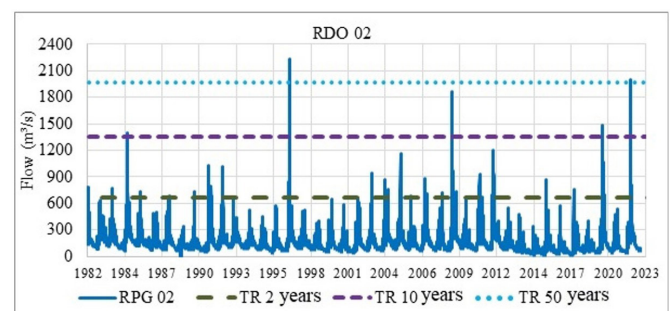


Figure 7. Doce River Station.

The three rivers have a considerable amount of medium sand, which shows uniformity. The coarse sand in the Doce River can be explained by the sediment load that the river water carries, which depends on the speed of the current and the diameter of the particles. The larger the diameter of the particles, the greater their weight, this can occur due to several factors, such as a decrease in the river's velocity gradient, smooth curves or an increase in the flooding area (Andrade et al., 2021).

Topographic data

The DEM was generated through data collected in the field (September/2021) and data acquired from other sources. Table 3 presents the coordinates and dates of the topobathymetric sections that were used from the ANA metadata catalog.

Figure 9 shows the confluence of the Carmo River with the Piranga River and the topobathymetric sections used to generate the DEM. The topobathymetric sections: CR-10, has an area of 29 m² and an average depth of 0.94 m; PG-71, has an area of 84 m² and an average depth of 0.90 m; DC-01, has an area of 314 m² and an average depth of 2.50 m. The difference in areas is related to the shape of the channel, in wide and deep channels the flow speed is slow. In narrow channels the flow speed is fast (Dietze et al., 2022).

In this region, the presence of several islands (Figure 10) was verified, which impact the flow and speed of the water current. Among them, those of a perennial nature, made up of rocks, and those of a temporary nature made up of sediments, which were formed as a result of flood events, stood out. The existence of these islands generated a complex scenario for the study of sediment transport, due to the multiplicity of variables involved and the difficulty in obtaining information. Another aspect to highlight

is that the confluence under study, although morphologically of type Y (Liu et al., 2019; Bilal et al., 2020; Yuan et al., 2021; Leli et al., 2023), presents perennial obstructions arising from rocky outcrops, makes this a peculiar type of confluence.

The DEM of the study area was made based on data from the topobathymetric sections and the slopes of the watercourses. The model was created with a spatial resolution of 1 m to better characterize the main and secondary channels of the rivers. We sought to represent the islands, as they are important in the study of flow and sediment transport. There was no need to represent the relief outside the main and secondary gutters, as they were not used in the simulation.

Models

2D hydrodynamic simulation

For the 2D hydrodynamic simulation, previously processed data was inserted into the HEC-RAS program. Manning roughness values were calculated for the main and secondary gutters, as proposed by Chow (1959).

The hydrodynamic simulation showed that at the confluence of the Carmo River with the Piranga River, the islands are obstacles to the flow. Figure 11 shows the flow velocity in the study area.

The highest speeds indicated by the red marking are in the sections funneled by the islands, which cause flow speeds to be greater than 1 m/s. These stretches are in the zone of maximum velocity, which is related to the junction of flows after the separation zone, which is commonly associated with increased frictional stress (Best, 1987; Biron et al., 1993, 1996; Boyer et al., 2006).

Low flow speeds are found on some banks and downstream of the islands, which are indicated by the black marking in Figure 11. The regions of low speed configure the stagnation zones. Stagnation zones occur due to the deflection of both flows at the junction and are associated with: increased pressure and depth; the decrease in flow velocity; and frictional stress (Best, 1987; Biron et al., 1996). The low-speed section on the left bank of the Doce River is explained by the natural barrier that dams the waters.

Figure 12 details the river flow at the confluence. The flow of the Carmo River is divided into 2 sections: A, with flow on the left, has 100% of the flow, while B, on the right, only occurs when the flow of the Carmo River is above 30 m³/s. This situation directly depends on the flow of the Piranga River. The Piranga River's flow is divided into 3 sections, shown in Figure 12. Section C drains 18% of the Piranga River's flow, while Section D drains 52% and Section E, 30%. This configuration is maintained up to the limit of 160 m³/s in the Carmo River and 210 m³/s in the Piranga River. From these flows, the islands begin to be flooded by waters.

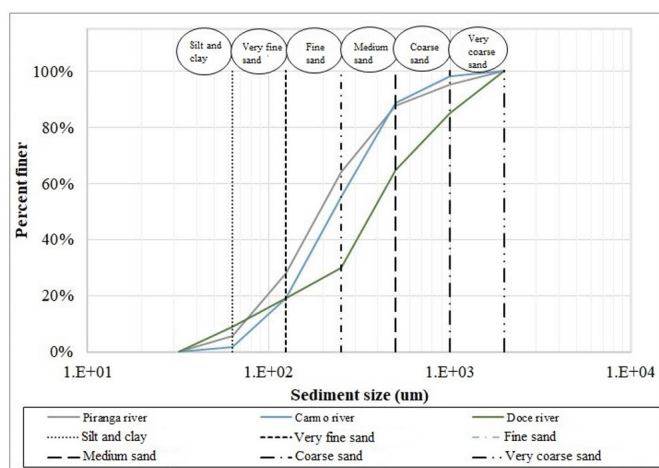


Figure 8. Granulometric distribution of rivers.

Table 3. Information on topobathymetric sections.

Section	Watercourses	Date	Latitude	Longitude
CR-10	Carmo River	01/17/2018	20° 16' 44.88" S	42° 55' 08.76" W
PG-71	Piranga River	11/29/2017	20° 16' 49.05" S	42° 54' 15.91" W
DC-01	Doce River	12/04/2017	20° 16' 21.15" S	42° 55' 08.59" W

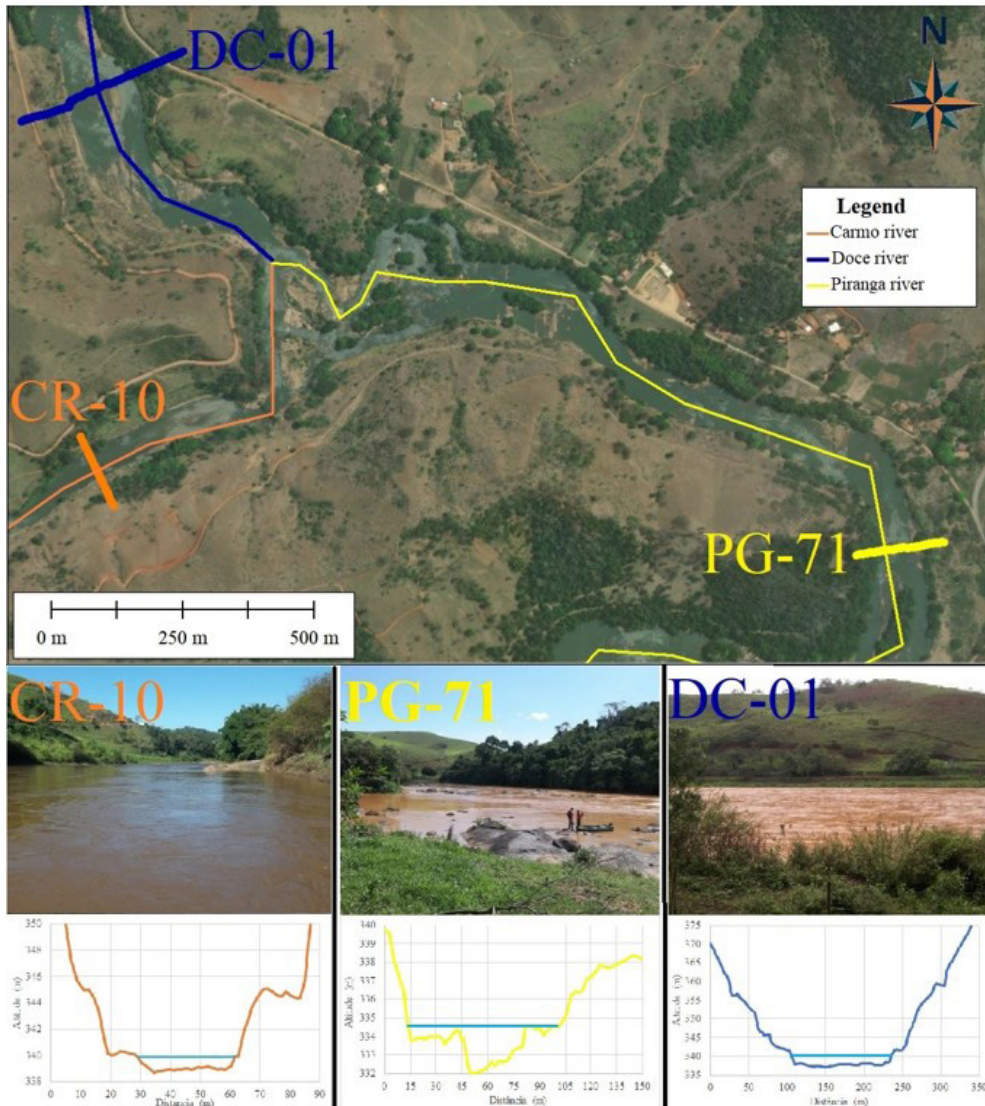


Figure 9. Confluence of the Carmo River with the Piranga River and topobathymetric sections. **Source:** Image (Google Earth, 2023); Photos (Brasil, 2023).

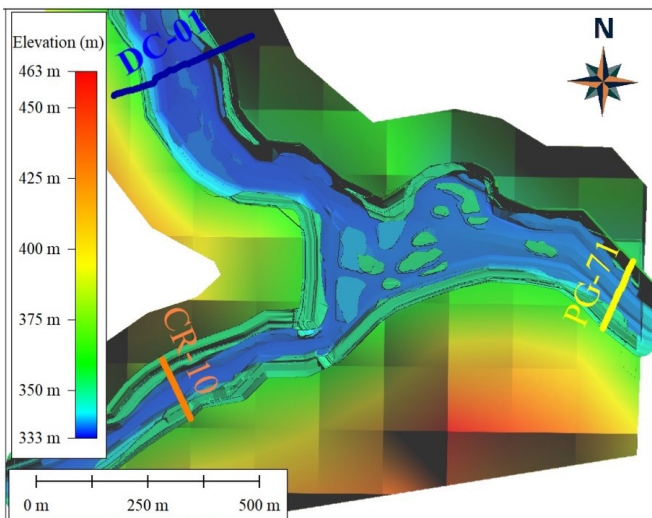


Figure 10. DEM of the confluence of the Carmo River with the Piranga River.

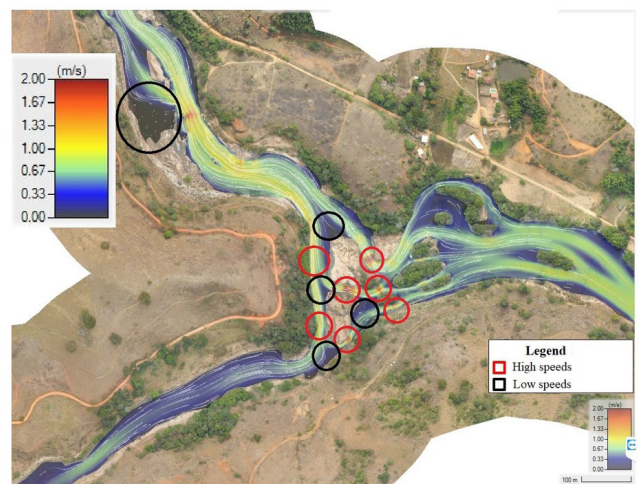


Figure 11. Orthophoto of the period from June to July 2022 with flow velocities at the confluence of the Carmo River with the Piranga River.

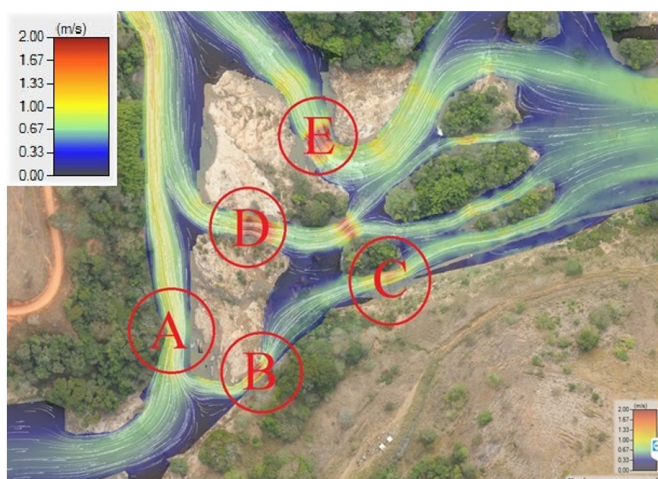


Figure 12. Orthophoto of the period from June to July 2022 with flow velocities at the confluence of the Carmo River with the Piranga River.

Figure 13 shows the flooded area on January 11, 2022, at 12 noon. The yellow marking shows two islands and part of the right bank of the Piranga River that were submerged, for an average height of 2 m. According to the DEM, there was no overflow of water into the secondary gutters due to the watercourse being embedded in the topography. The islands are constantly flooded from December to February, as the sum of the flows of the Carmo River and the Piranga River is often greater than 160 m³/s.

The black marking was placed to show the usual (normal) limit of the watercourse in comparison to the flood spot area. It was observed that there are no large overflows due to the fit of the watercourse into the topography in the study area, as previously mentioned.

No study was found with hydrodynamic simulations specifically in the researched area. Machado (2017) and Almeida (2019) simulated the propagation of the flood wave caused by the rupture of the Fundão dam up to 10 km downstream of the disaster. The studied area is 80 km downstream of the Fundão dam and has a different simulated period, making it incompatible for comparisons.

Based on the DEM (Figure 10) and the topobathymetric sections (Figure 9), it is observed that the topography is embedded in the watercourse. Therefore, even though the flow of the January flood event was greater than the flow that occurred in the Mariana – MG disaster, a similarity in the flood area is expected. The flood area varied little and the runoff speed fluctuated more compared to the Mariana – MG disaster. The simulation showed that the area flooded by the Mariana – MG disaster was 2.48 x 10⁶ m², 4% smaller than the area flooded in the January 2022 event (Figure 14). No image record of the day of the disaster was found at this

The floodplain from the Mariana disaster (Figure 14) was provided by the RENOVA Foundation, which carries out studies to minimize and understand the disaster that occurred. This stain confirms that the banks are embedded in the watercourses. Even though the events had different amplitudes, there were no significant variations in the floodplain areas.

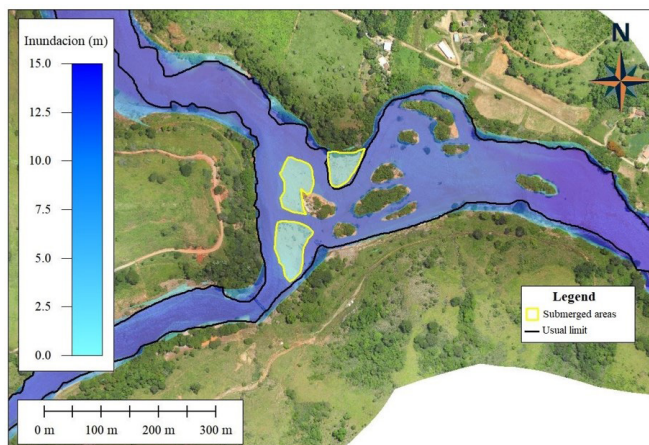


Figure 13. Orthophoto of the period January to March 2022 with the flood patch from the January 2022 event.

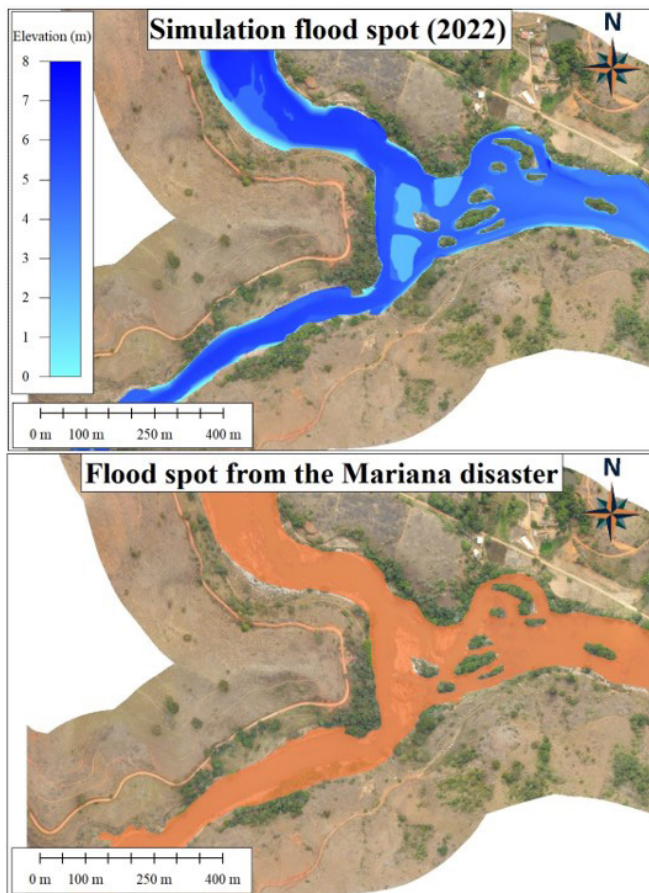


Figure 14. Orthophoto of the period from June to July 2022 with the flood spots from the Mariana -MG disaster (2015) and the January 2022 event.

This study corroborates those of Dasallas et al. (2019), Hagg et al. (2021) and Shaikh et al. (2023) among others, who state that in funneled areas the flow speed increases in relation to other sections.

2D sediment transport simulation

After the 2D hydrodynamic simulation, sediment data was inserted into the HEC-RAS program. Figure 14 shows the places where sediment deposition and erosion occurred at the confluence of the Carmo River with the Piranga River (which constitutes the official starting point of the Rio Doce) after the January 2022 flood event.

The 2D sediment transport simulation showed that in the period from January 1 to March 30, 2022, there was more sediment deposition than erosion. Figure 15 shows in blue, the deposition of sediments, and in red, the places where erosion occurred.

The quantitative analysis of the sediments that entered and left the study area during the simulated period is represented in Table 4. The Carmo river brought $3.1 \times 10^{-2} \text{ hm}^3$ of sediment, while the Piranga river brought $8.6 \times 10^{-2} \text{ hm}^3$. In addition to these sediments that entered the area, there was erosion of $5.8 \times 10^{-2} \text{ hm}^3$, totaling $17.5 \times 10^{-2} \text{ hm}^3$ of sediment transported. Of these, a portion of $8.6 \times 10^{-2} \text{ hm}^3$ was deposited internally, while the remainder, 8.9×10^{-2} cubic hectometers, was transported outside the study area.

A predominance of the sedimentation process in relation to erosion was observed, which results in significant implications, which include an increase in the frequency and intensity of floods, since the space available for water flow has been reduced due to the accumulation of sediments (Pakam et al., 2023). Furthermore, sediment accumulation has a direct impact on aquatic ecosystems, suffocating resident organisms and resulting in a decrease in biodiversity and disruption of food chains (Darko et al., 2021).

No study was identified in the literature that was dedicated to carrying out simulations related to sediment transport at confluences in the research area of this study. The sediment retention values presented in Table 4 will be compared with estimated values (Palu, 2019) for the first reservoir downstream of the rupture site.

In the study by Palu (2019), the efficiency of sediment retention in the Risoleta Neves reservoir during the Mariana disaster, MG, was 60%, corresponding to a volume of 7 hm^3 , which resulted in a loss of 17% of the total reservoir volume.

The sediment retention efficiency at the confluence of the Piranga and Carmo rivers was approximately 50% (Table 4) during the January 2022 flood event. This value is comparable to the 60% obtained above for the reservoir, indicating the importance of this confluence for the sediment balance. Figure 15 shows that the islands play an important role in sediment retention, retaining much of the sediment that entered and eroded during the event. This confluence behaved in a similar way to a dam, which corroborates the idea that “Y” shaped confluences with the presence of rocky outcrops together with reservoirs are effective in retaining sediment.

Figure 16 shows some areas of sediment deposition. These areas of sediment accumulation coincide with those indicated by low hydrodynamics (Fig. 10), and may present reverse flow directions as shown by the stagnation zones in this figure. as anticipated in other regions (Best, 1987, 1988; Best & Rhoads, 2008; Bennert et al., 2017).

In Figure 16, areas A1 and A2 correspond to 2 morphological features, indicated by Best (1986) and Best & Rhoads (2008):

- I) Probable landslide area formed at the mouth of both channels;
- II) Deposition of sediments within a stagnation zone at the corner of the junction forming a lateral bar. Rhoads (2006), Best (1988), Turra et al. (1999), Best & Rhoads (2008) and Stevaux et al. (2009) consider that the origin of the sidebars is linked to the flow separation zone, which coincides with area A.

According to Mosher & Martini (2002) and Rhoads (2006), these bars develop during flood events and are characterized by the presence of coarse grain size on the surface. Another characteristic of these bars, described by Rhoads & Kenworthy (1995) and Rhoads (2006), is the formation of a fine-grained ridge that marks the threshold of the flow separation zone. The 2D sediment transport model calculated that in this area there was an average sediment deposition of 0.40 m.

Areas B (tip of the island) and C (Figure 16) are stagnation zones, resulting from the islands. After the stagnation zone, the flow velocity increases (Figure 11), in agreement with the studies by Baranya et al. (2015), Leite Ribeiro et al. (2016), Santos & Stevaux (2017) and Shukla et al. (2022b). In line with the study by Miyawaki et al. (2010) the flow junction created alternating vortices similar to von Kármán vortices, in areas B and C of Figure 16.

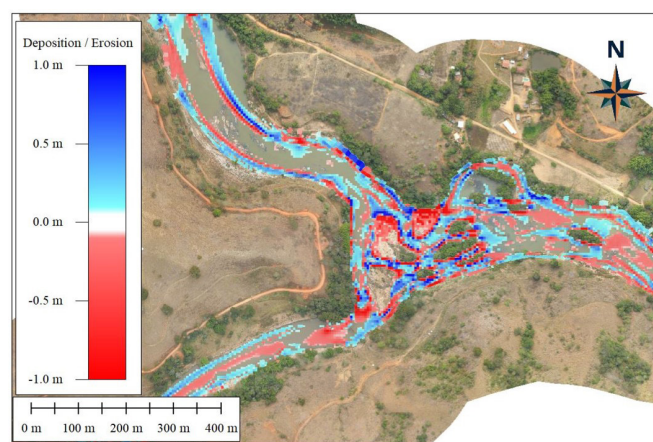


Figure 15. Orthophoto of the period from June to July 2022 with the areas of sediment deposition and erosion at the confluence of the Carmo River with the Piranga River.

Table 4. Sediment budget.

	Sediment Input (hm^3)	Sediment Retention (hm^3)
Carmo River (Upstream)	3.1×10^{-2} (18%)	
Piranga River (Upstream)	8.6×10^{-2} (49%)	
Erosion	5.8×10^{-2} (33%)	
Deposition		8.6×10^{-2} (49%)
Sediment Output		
Doce River (Downstream)		8.9×10^{-2} (51%)

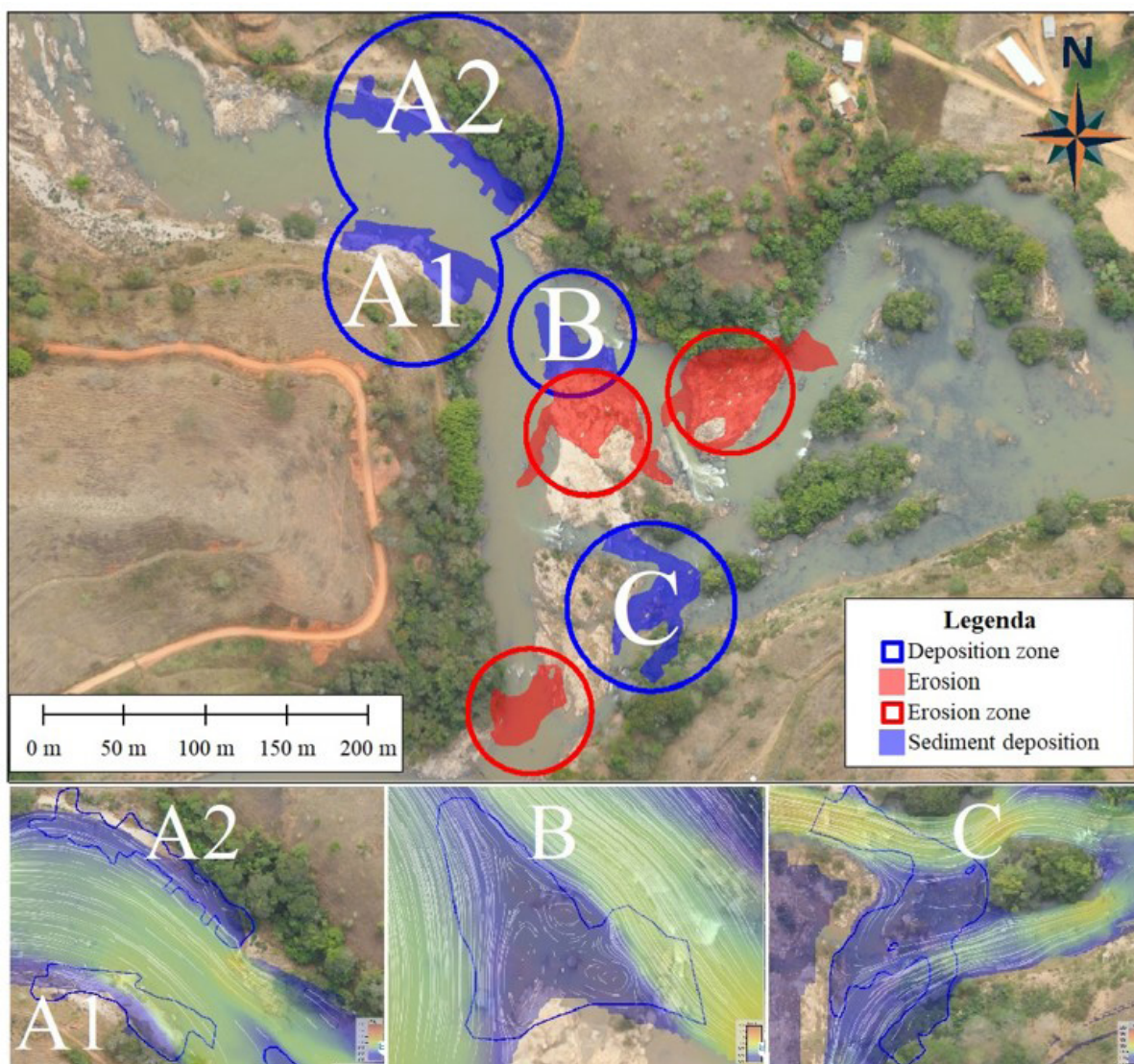


Figure 16. Orthophoto from June to July 2022 with areas of sediment deposition in the shear zone with flow velocity.

The 2D sediment transport model calculated that in these areas there was deposition sediment average of 0.60 m.

Figure 17 shows the erosion areas. The erosion process occurred on the islands due to high flows from the January 2022 event that surpassed the surface of the islands, dragging sediments. In the central part of the watercourses, the islands made drainage difficult, causing the waters to bypass these islands. It then substantially increased the speed of flow in the bypassed areas, consequently excavating the river bed.

The erosions depicted in areas D (Figure 18) occurred because of the January 2022 flood event. These areas were submerged by high-velocity waters, causing sediments to detach from the soil. The model calculated that area D had an average erosion of 0.30 m and area E of 0.40 m. Figure 18 shows a profile of area D, where the blue line represents the surface before the 2022 event and the red line after the 2022 event, it is clear that there was erosion. These areas are devoid of vegetation, (Figure 12) which corroborates the result presented, and may also indicate constant flooding.

Area F shows an excavation area, caused by a lateral choke. This excavation area is related to the junction angle and the increase in flow velocity (Figure 11), which coincides with the studies by Mosley (1979) and Best (1988). According to Bryan & Kuhn (2002), the excavation zones at the confluences (type Y), similar to this study, are symmetrical, where the excavation zone is practically located in the central part of the watercourse. The excavation area is characterized by turbulence along the shear layer between the flows, leading to rotation of sediments in the surrounding area or cleaning the excavation area (Atkinson, 1987; Roy et al., 1988; Boyer et al., 2006; Shukla et al., 2022b). Mosley (1976), Best (1988) and Santos & Stevaux (2017), describe that the depth of the excavation zone is closely related to the confluence angles, and that at acute angles the depth tends to be deeper in relation to the watercourse channel. 2D sediment calculated that there was an average excavation of 0.70 m in this area, making the channel deeper.

The 2D sediment transport simulation showed that the extreme flooding event of January 2022 eroded part of some islands and hydrodynamically deposited sediment on the banks.

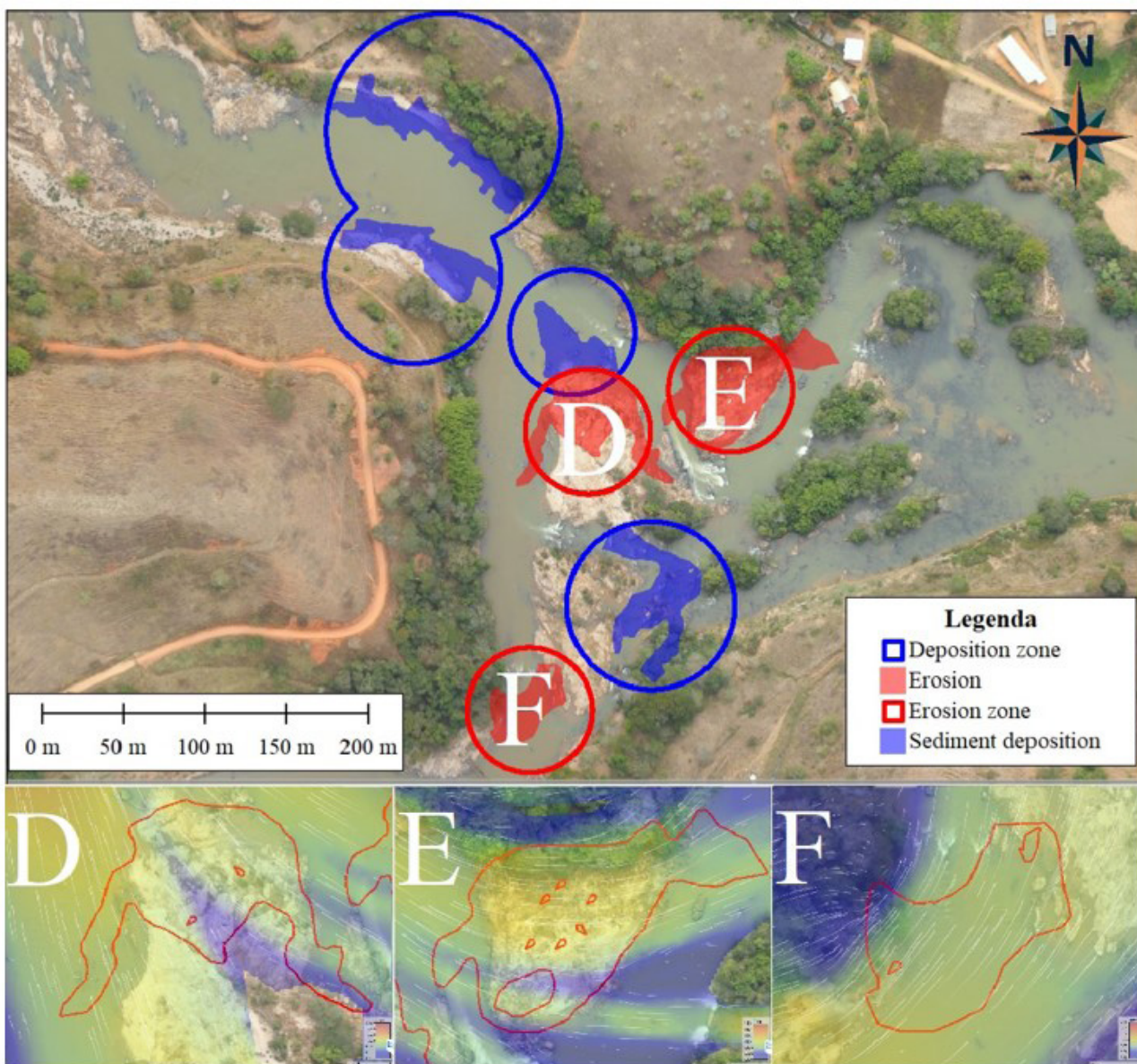


Figure 17. Orthophoto of the period from June to July 2022 with areas of sediment erosion in the shear zone with flow velocity.

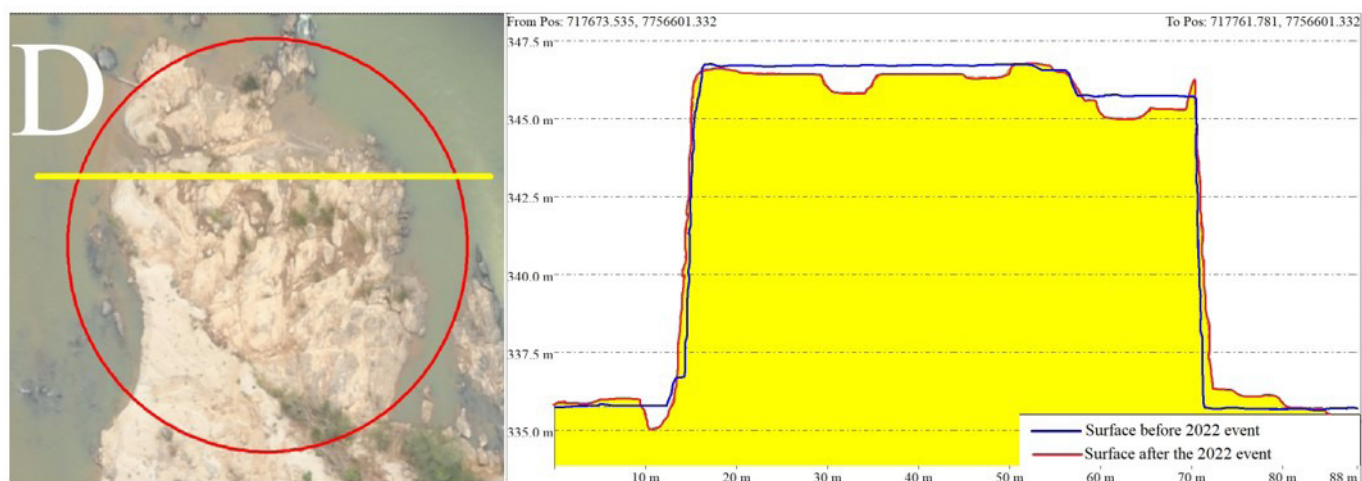


Figure 18. Profile of erosion area D.

The results indicate that extreme events have the capacity to change the morphology of confluences. Furthermore, there is a constant change in the morphology of the confluences mainly due to the deposition of sediments which is superior to erosion.

No study was found with simulations of sediment transport at confluences in this area. However, there is agreement with the study by Palu (2019), that sediment parameters significantly influence the volume of sediment mobilized in the Risoleta Neves reservoir, which is downstream of the study area.

Magliulo et al. (2021), analyzed the adjustments of a channel over 140 years in response to extreme floods on the Tammaro River, in southern Italy, and showed that extreme floods can in a very short time produce morphological changes comparable to adjustments long-term channel. Shrestha et al. (2020), analyzed hydrological and morphological changes in the Chindwin River, in Miami, and showed the occurrence of morphological changes resulting from extreme events in climate change scenarios. Both studies confirm that extreme events can change the morphology of watercourses, as observed here.

Calibration and evaluation of models

2D hydrodynamic simulation

The calibration of the 2D hydrodynamic model was done using the Manning coefficient adjustment. These coefficients were adjusted between 0.030 and 0.070 for the main flume and 0.09 to 0.14 for the secondary flume, to find the best fit between the simulated hydrograph and that of the downstream monitoring station. The coefficient of 0.035 was used for the main gutter and 0.11 for the secondary gutter according to the methodology of Rangel (2021).

Using orthophotos, the area of the flood spot was assessed. The flood spot was identified, which has an area of 222 thousand square meters, highlighting 9 islands that were not submerged by water. The simulation's flood spot was also vectorized, which has an area of 258 thousand square meters, 16% larger than the area of the spot created by the orthophoto. Figure 19 shows the comparison of the images, since the flood spot generated by the simulation does not have the same precision as the orthophoto from January 2022 (during the event). This difference is due to the limitations of topography and bathymetry data.

To verify the reach of the flood spot, the yellow area in Figure 19 was investigated to highlight the reach of the spot. Figure 20, photo taken in August 2023, shows the primary trough and the beginning of the secondary trough confirming the reach of the floodplain from the 2D hydrodynamic simulation, which was similar to the beginning of the secondary trough indicated by Figure 19.

Figure 21 shows the comparison of the hydrographs, simulated and observed, by the monitoring station RDO 02 – Rio Doce (Figure 7). The comparison of the hydrographs, simulated and observed, shows that the hydrograph of the RDO 02 station, which is downstream of the confluence and the

Risoleta Neves plant, recorded a maximum flow of 2000 m³/s on January 11, 2022, while the simulation recorded a flow of 1480 m³/s. In agreement with the work of Dias et al. (2018), Palu (2019) and Figueiredo et al. (2019), the dam at the Risoleta Neves Hydroelectric Power Plant plays a role in dampening extreme events, as was seen in the Mariana disaster – MG.

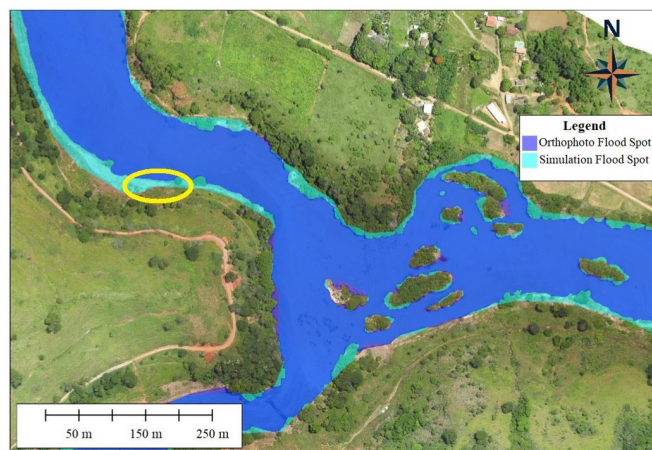


Figure 19. Orthophoto from the period January 2022 with comparisons of the flood spots generated by the orthophoto taken during the event and by the 2D hydrodynamic simulation.



Figure 20. Photo taken from the A2 deposition area, in August 2023.

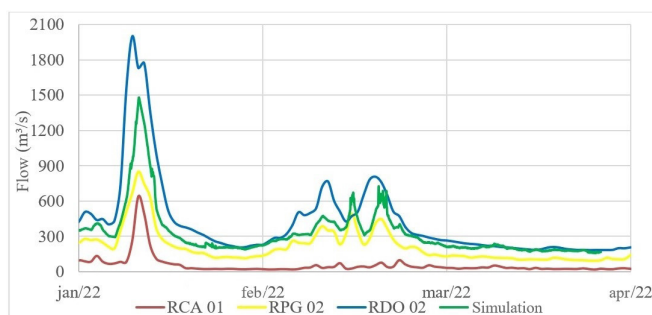


Figure 21. Comparison of simulated and observed hydrographs.

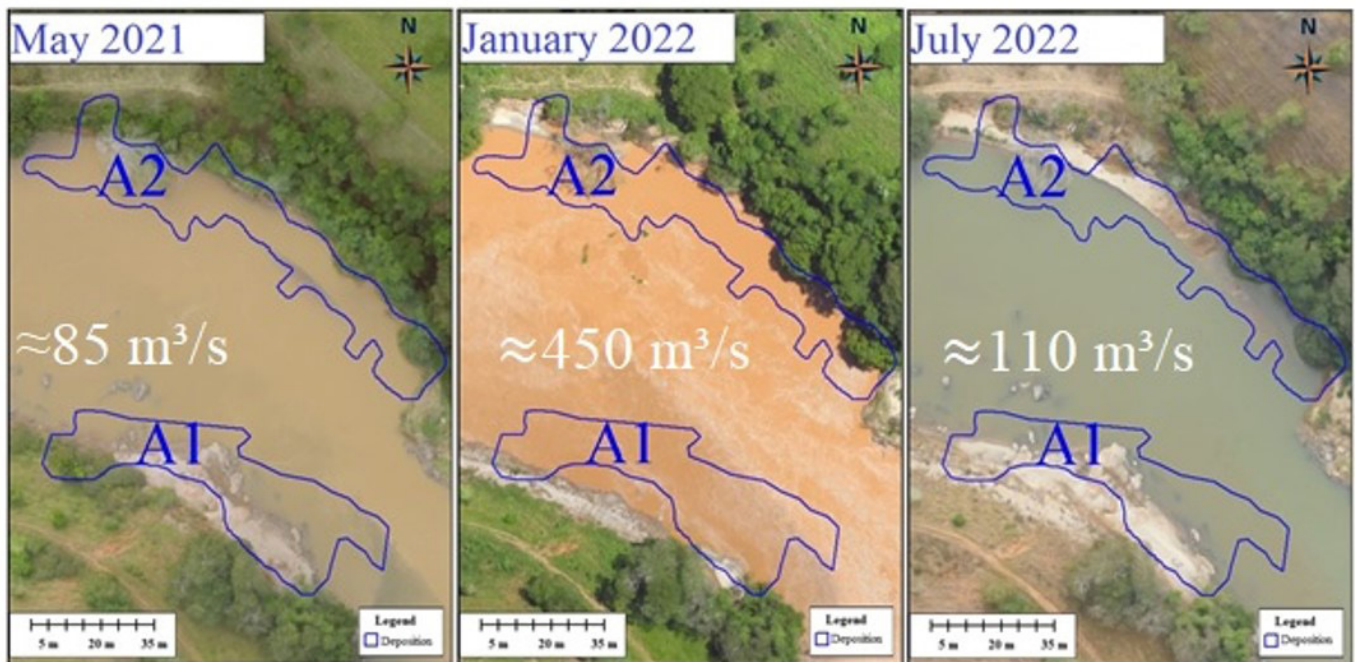


Figure 22. Comparison of orthophotos from before, during and after the 2022 flood event.

The sum of the flows from the RCA 01 stations (Figure 5) – Carmo river and the RPG 02 station (Figure 6) – Piranga river which are upstream of the confluence was $1486 \text{ m}^3/\text{s}$, and the flow recorded by the simulation was $1480 \text{ m}^3/\text{s}$. The date of recording this flow is January 11, 2022, the same date as the maximum flows at the stations, with a delay of 3 hours. By comparing the maximum flows of the station that are upstream of the confluence with the flow recorded by the simulation, the model evaluation was considered adequate, due to the small difference in flow and peak time between them.

2D sediment transport simulation

The calibration of the 2D sediment transport model was carried out in the HEC-RAS program, adjusting the transport function according to Brunner (2020) and Gudgeirsdóttir (2023), for rivers from 30 to 100m the recommended value is 10 m.

To evaluate the 2D sediment transport simulation, orthophotos were used to highlight changes in the morphology of the confluence after the January 2022 flood event.

Figure 22 shows the comparison of orthophotos: before the event, during the event and after the January 2022 event, in area A2 (Figure 15). There were changes in the morphology of the channel, in the same location indicated by the 2D sediment transport simulation.

Figure 23 shows a photo taken in August 2023 of the A2 deposition area (Figure 16). There is evidence that there was hydrodynamic deposition, which can be proven by the amount of sand sedimented in the ravine. This hydrodynamic deposition may have occurred because of the January 2022 flood that reached a height of 4.6 m above the mean level (Figure 13) with a flow speed below 0.5 m/s (Figure 11).



Figure 23. Photo taken from the A2 deposition area in August 2023.

In Figure 24, the topobathymetric section surveyed in the field, on the Doce River, was compared with the orthophotos before and after the January 2022 flood event. The first orthophoto has an extension of 101 m while the following orthophoto has an extension of 101.5 m. According to the orthophotos, there was no significant change in the morphology of the margins. The simulation showed the same results.

The 2D sediment transport simulation (Figure 25) shows that, in the topobathymetric section, there was a sediment deposition between the distance 80 m and 101 m, of approximately 0.35 m. This can be explained by Figure 11, which shows the speed in this section, which is relatively low compared to the other sections of the section. There were no changes in the rest of the section.

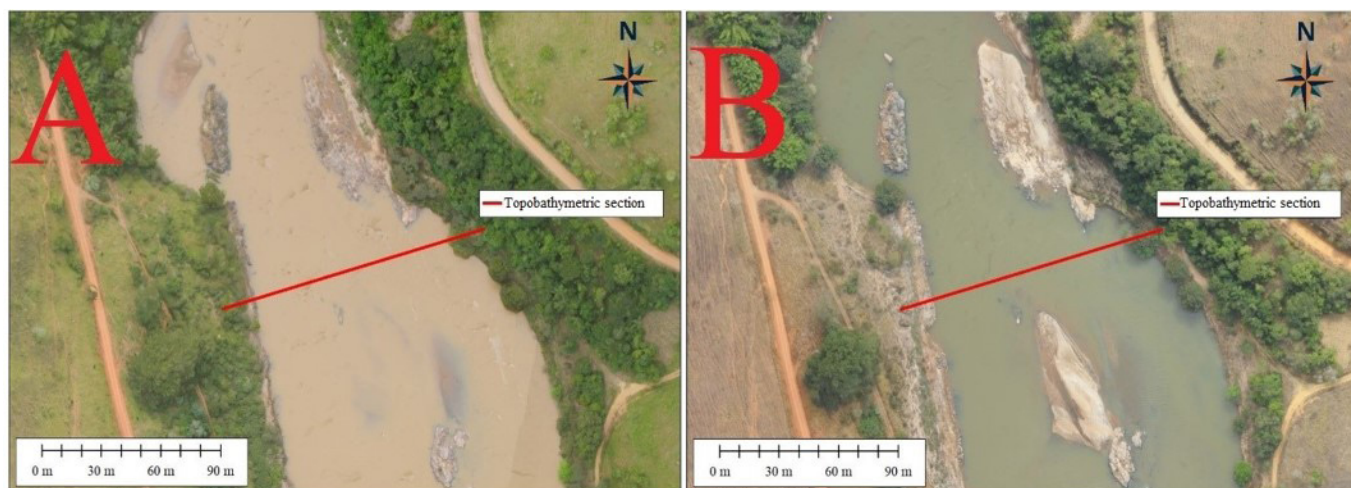


Figure 24. Orthophotos with the topobathymetric sections of the Doce River, (A) Orthophoto (before the event) period from April to May 2021; and (B) Orthophoto (after the event) period from June to July 2022.

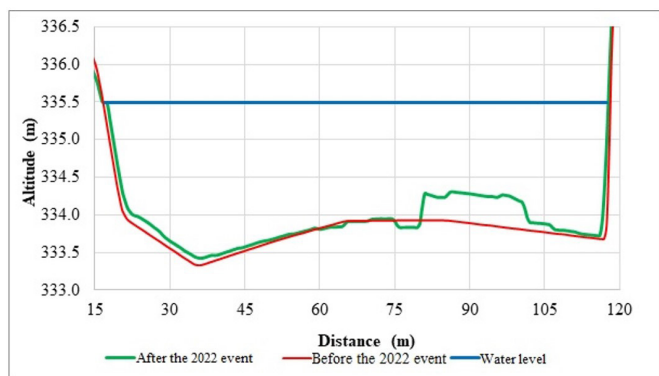


Figure 25. Topobathymetric sections of the 2D sediment transport simulation, in the HEC-RAS program.

CONCLUSIONS

According to the analyses of the field observations and remote sensing data, combined with hydrodynamic and sediment transport modelling from the bidimensional (2-D) hydrological engineering center-river analysis system (HEC-RAS) model, we evaluated changes in hydromorphological conditions due a flood depth with 50 years return period. The study area encompasses a river confluence which is the official milestone of the beginning of the Rio Doce, one of the rivers in the world with the greatest concentration of studies aimed at its restoration, after having suffered one of the biggest disasters due to the collapse of a tailings dam. The main conclusions are as follows:

- 1) The REC-HAS model skills showed good performance in reproducing sediment transport during an extreme hydrological pulse, as qualitatively verified from high resolution images and field data.
- 2) The simulation results of the sediment budgets have shown that this confluence has a regional significance to net sediment transport functioning as an enhanced sediment retention area (sediment storage), with approximately 50% retention rate, comparable to that of the reservoirs.

The numerical model calculations show that the sediment transport value downstream of the confluence is $8,9 \times 10^2 \text{ hm}^3$ or 152 tons, considering a wet sand density of 1.7 kg/m^3 , while the corresponding sedimented value (sediment storage) is $8,6 \times 10^2 \text{ hm}^3$ or 147 tons. Since the estimated suspended sediment flux at the Doce river was $11 \times 10^6 \text{ ton/year}$ (Lima et al., 2005), the amount trapped here during the event is considerable. The retention behavior was determined not only by the geometry of the confluence but also by the presence of a rocky bed.

- 3) Bed and bank material data gradation curves shown that small sand particles dominate in upstream while medium sand particles dominate at downstream of the confluence. The resultant bars or islands were caused by sediment deposition due to low velocities and/or flow recirculation. (Figure 8, 14 and 15)
- 4) 2-D HEC-RAS model proved to be efficient in depicting the sedimentation and scour occurring in the side slope of a river cross-section, as corroborated by the cross-section measures before and after the event. Geometric changes in cross-section indicated that sediment distribution was not uniform throughout the study reach and that right side of the river boundary was a strength deposition area. (Figure 21 and 22).

The results presented here have the potential to indicate the river reaches with remarkable sediment deposition. These reaches deserve some hydraulic engineering intervention, in order to prevent the sediments trapped in this area to be transported downstream during hydraulic pulses in years to come. Overall, HEC-RAS 2-D model shown to be a very useful tool for forecasting morphological changes in near future in river banks, which would ultimately be useful for planning and execution of River Doce restoration issue.

ACKNOWLEDGEMENTS

The authors acknowledge support from the FAPEMIG/ Fundação Renova (Project APQ 00405-19) and the National Council for Scientific and Technological Development of Brazil (CNPq).

REFERENCES

- Alaska Satellite Facility – ASF. (2023). Retrieved in 2023, December 1, from <https://search.asf.alaska.edu/#/>.
- Almeida, B. C. M. D. (2019). *Retroanálise da propagação decorrente da ruptura da barragem de Fundão através do modelo numérico HISTAV* (Monografia). Universidade Federal de Minas Gerais, Belo Horizonte. Retrieved in 2023, December 1, from https://www.researchgate.net/profile/Aloysio-Saliba/publication/340647478_Retroanalise_da_propagacao_decorrente_da_ruptura_da_barragem_do_Fundao_atraves_do_modelo_numerico_HISTAV_Retroanalysis_of_Fundao_dam_break_using_the_HISTAV_model/links/61923c9707be5f31b78272ca/Retroanalise-da-propagacao-decorrente-da-ruptura-da-barragem-do-Fundao-atraves-do-modelo-numerico-HISTAV-Retroanalysis-of-Fundao-dam-break-using-the-HISTAV-model.pdf
- Alves, F. H. B. (2017). *Sistema de previsão de enchentes: integração de modelos de previsão de chuva, simulação hidrológica e hidrodinâmica* (Dissertação de mestrado). Universidade Federal de Pernambuco, Recife. Retrieved in 2023, December 1, from <https://repositorio.ufpe.br/handle/123456789/26314>.
- Andrade, A. C. F. (2020). *Mapeamento e caracterização do sistema rio-planície da Amazônia central via sensoriamento remoto e modelagem hidráulica* (Tese de doutorado). Instituto de pesquisas Hidráulicas, Universidade Federal do Rio Grande do Sul, Porto Alegre. Retrieved in 2023, December 1, from <https://lume.ufrgs.br/bitstream/handle/10183/211269/001115515.pdf?sequence=1&isAllowed=y>
- Andrade, L. N. P. D. S., Cunha-Santino, M. B., & Souza, C. A. (2021). Aporte de sedimentos a montante da uhe colider, no médio curso do Rio Teles Pires-Mato Grosso. *Revista Equador*, 10(2), 270-297. <http://dx.doi.org/10.26694/equador.v10i2.12781>.
- Anim-Gyampo, M., Anornu, G. K., Appiah-Adjei, E. K., & Agodzo, S. K. (2019). Quality and health risk assessment of shallow groundwater aquifers within the Atankwidi basin of Ghana. *Groundwater for Sustainable Development*, 9, 100217. <http://dx.doi.org/10.1016/j.gsd.2019.100217>.
- Atkinson, M. J. (1987). Low phosphorus sediments in a hypersaline marine bay. *Estuarine, Coastal and Shelf Science*, 24(3), 335-347. [http://dx.doi.org/10.1016/0272-7714\(87\)90054-0](http://dx.doi.org/10.1016/0272-7714(87)90054-0).
- Azarang, F., & Bajestan, M. S. (2015). Simulating the erosion and sedimentation of Karun Alluvial River in the Region of Ahvaz (southwest of Iran). *American Journal of Engineering Research*, 4(7), 233-245. Retrieved in 2023, December 1, from <https://www.academia.edu/download/47617691/ZD04702330245.pdf>
- Baranya, S., Olsen, N. R. B., & Józsa, J. (2015). Flow analysis of a river confluence with field measurements and RANS model with nested grid approach. *River Research and Applications*, 31(1), 28-41. <http://dx.doi.org/10.1002/rra.2718>.
- Batista, J. T. P. D. P. (2022). *Obtenção de mapas de inundação a partir de diferentes tempos de retorno: estudo de caso da cidade de Piranga-MG* (Trabalho de conclusão de curso). Universidade Federal de Ouro Preto, Ouro Preto. Retrieved in 2023, December 1, from <http://www.monografias.ufop.br/handle/35400000/4666>.
- Bennert, A., Leli, I. T., Fernandez, O. V. Q., & Hayakawa, E. H. (2017). Caracterização geomorfológica em confluência: estudo de caso dos rios Paraná\Piquiri. *Os Desafios da Geografia Física na Fronteira do Conhecimento*, 1, 6335-6343. <http://dx.doi.org/10.20396/sbgfa.v1i2017.2521>.
- Berghout, A., & Meddi, M. (2016). Sediment transport modelling in wadi Chemora during flood flow events. *Journal of Water and Land Development*, 31(1), 23-31. <http://dx.doi.org/10.1515/jwld-2016-0033>.
- Best, J. L. (1986). The morphology of river channel confluences. *Progress in Physical Geography*, 10(2), 157-174. <http://dx.doi.org/10.1177/030913338601000201>.
- Best, J. L. (1987). Flow dynamics at river channel confluences: implications for sediment transport and bed morphology. *Sedimentology*, 39, 27-35. Retrieved in 2023, December 1, from https://archives.datapages.com/data/sepm_sp/SP39/Flow_Dynamics_at_River.htm
- Best, J. L. (1988). Sediment transport and bed morphology at river channel confluences. *Sedimentology*, 35(3), 481-498. <http://dx.doi.org/10.1111/j.1365-3091.1988.tb00999.x>.
- Best, J. L., & Rhoads, B. L. (2008). Sediment transport, bed morphology and the sedimentology of river channel confluences. In S. P. Rice, A. G. Roy & B. L. Rhoads (Eds.), *River confluences, tributaries and the fluvial network* (pp. 45-72). Hoboken: Wiley. <http://dx.doi.org/10.1002/9780470760383.ch4>.
- Best, J. L., & Roy, A. G. (1991). Mixing-layer distortion at the confluence of channels of different depth. *Nature*, 350(6317), 411-413. <http://dx.doi.org/10.1038/350411a0>.
- Bilal, A., Xie, Q., & Zhai, Y. (2020). Flow, sediment, and morphodynamics of river confluence in tidal and non-tidal environments. *Journal of Marine Science and Engineering*, 8(8), 591. <http://dx.doi.org/10.3390/jmse8080591>.
- Biron, P., Roy, A. G., & Best, J. L. (1996). Turbulent flow structure at concordant and discordant open-channel confluences. *Experiments in Fluids*, 21(6), 437-446. <http://dx.doi.org/10.1007/BF00189046>.
- Biron, P., Roy, A., Best, J. L., & Boyer, C. J. (1993). Bed morphology and sedimentology at the confluence of unequal depth channels. *Geomorphology*, 8(2-3), 115-129. [http://dx.doi.org/10.1016/0169-555X\(93\)90032-W](http://dx.doi.org/10.1016/0169-555X(93)90032-W).
- Boyer, C., Roy, A. G., & Best, J. L. (2006). Dynamics of a river channel confluence with discordant beds: flow turbulence, bed load sediment transport, and bed morphology. *Journal of Geophysical Research*, 111(F4), 2005JF000458. <http://dx.doi.org/10.1029/2005JF000458>.

- Brasil. Agência Nacional de Águas e Saneamento Básico – ANA. (2023). *Catálogo de metadados da ANA*. Brasília. Retrieved in 2023, December 1, from <https://metadados.snirh.gov.br/geonetwork/srv/por/catalog.search#/home>
- Brunner, G. W. (2020). *HEC-RAS hydraulic reference manual*. Retrieved in 2023, December 1, from <https://www.hec.usace.army.mil/confluence/rasdocs/ras1dtechref/latest>
- Bryan, R. B., & Kuhn, N. J. (2002). Hydraulic conditions in experimental rill confluences and scour in erodible soils. *Water Resources Research*, 38(5), 21-1. <http://dx.doi.org/10.1029/2000WR000140>.
- Calle, M., Alho, P., & Benito, G. (2017). Channel dynamics and geomorphic resilience in an ephemeral Mediterranean river affected by gravel mining. *Geomorphology*, 285, 333-346. <http://dx.doi.org/10.1016/j.geomorph.2017.02.026>.
- Campana, K. D. S. (2022). Simulação de transporte de sedimentos em trecho do rio Doce (ES) utilizando modelagem computacional. *Destarte*, 11(2), 95-130. Retrieved in 2023, December 1, from <https://estacio.periodicoscientificos.com.br/index.php/destarte/article/download/1505/1249>
- Chen, Y., & Falconer, R. A. (1992). Advection-diffusion modelling using the modified QUICK scheme. *International Journal for Numerical Methods in Fluids*, 15(10), 1171-1196. <http://dx.doi.org/10.1002/flid.1650151003>.
- Chow, V. T. (1959). *Open-Channel Hydraulics*. New York: McGraw-Hill Book Company. Retrieved in 2023, December 1, from <https://heidarpour.iut.ac.ir/sites/heidarpour.iut.ac.ir/files/u32/open.pdf>.
- Cienciala, P., & Pasternack, G. B. (2017). Floodplain inundation response to climate, valley form, and flow regulation on a gravel-bed river in a Mediterranean-climate region. *Geomorphology*, 282, 1-17. <http://dx.doi.org/10.1016/j.geomorph.2017.01.006>.
- Coelho Filho, J. A. P., Matos, A. J. S., & Davis, E. G. (2022). *Sistema de alerta hidrológico da bacia do rio Doce: relatório técnico de operação do ano hidrológico 2021/2022*. Belo Horizonte: CPRM. Retrieved in 2023, December 1, from http://dspace.cprm.gov.br/bitstream/doc/23324/1/SAH_doce_relatorio%20anual_2022.pdf
- Copeland, R. R., & Thomas, W. A. (1989). *Lower Mississippi River Tarbert Landing to East Jetty Sedimentation Study: numerical model investigation*. Vicksburg: US Army Waterways Experimental Station. Retrieved in 2023, December 1, from <https://apps.dtic.mil/sti/citations/ADA254685>.
- Corum, Z., Jones, K., & Dahl, T. (2023). *Practical evaluation of USACE sediment models on the Lower White River in Washington State: case study of the Countyline Levee Setback project*. SEDHYD, Inc. Retrieved in 2023, December 1, from <https://www.sedhyd.org/2023Program/1/233.pdf>
- Damte, F., Mariam, B., Ayana, M. T., Lohani, T. K., Dhiman, G., & Shabaz, M. (2021). Computing the sediment and ensuing its erosive activities using HEC-RAS to surmise the flooding in Kulfo River in Southern Ethiopia. *World Journal of Engineering*, 18(6), 948-955. <http://dx.doi.org/10.1108/WJE-01-2021-0002>.
- Darko, H. F., Karikari, A. Y., Duah, A. A., Akurugu, B. A., Mante, V., & Teye, F. O. (2021). Effect of small-scale illegal mining on surface water and sediment quality in Ghana. *International Journal of River Basin Management*, 21(3), 1-12.
- Das, B., & Senthil Vadivel, T. (2022). Sediment transport modelling in stream flow by HEC-RAS model: a state-of-the-art. In P. G. Kumar, K. V. L. Subramaniam, S. M. Santhakumar, & D. N. Satyam (Eds.), *Recent advances in civil engineering* (Lecture Notes in Civil Engineering, No. 233). Singapore: Springer.
- Dasallas, L., Kim, Y., & An, H. (2019). Case study of HEC-RAS 1D–2D coupling simulation: 2002 Baeksan flood event in Korea. *Water*, 11(10), 2048. <http://dx.doi.org/10.3390/w11102048>.
- Dawson, K. (2021). *Intervention: sedimentary justice: a planetary politics of shifting sediment*. Antipode Online. Retrieved in 2023, December 1, from <https://antipodeonline.org/2021/07/12/sedimentary-justice/>
- Dias, C. A., da Costa, A. S. V., Guedes, G. R., de Matos Umbelino, G. J., de Souza, L. G., Alves, J. H., & Silva, T. G. M. (2018). Impactos do rompimento da barragem de Mariana na qualidade da água do rio Doce. *Revista Espinhaço*, 7(1), 21-35. Retrieved in 2023, December 1, from <http://hdl.handle.net/1843/54212>
- Dietze, M., Bell, R., Ozturk, U., Cook, K. L., Andermann, C., Beer, A. R., Damm, B., Lucia, A., Fauer, F. S., Nissen, K. M., Sieg, T., & Thielen, A. H. (2022). More than heavy rain turning into fast-flowing water: a landscape perspective on the 2021 Eifel floods. *Natural Hazards and Earth System Sciences*, 22(6), 1845-1856. <http://dx.doi.org/10.5194/nhess-22-1845-2022>.
- Duan, Y., Wang, C. Y., Zheng, C. Y., Wu, B. X., & Zheng, G. D. (2008). Geochemical study of crude oils from the Xifeng oilfield of the Ordos basin, China. *Journal of Asian Earth Sciences*, 31(4-6), 341-356. <http://dx.doi.org/10.1016/j.jseaes.2007.05.003>.
- Edmonds, D. A., Toby, S. C., Siverd, C. G., Twilley, R., Bentley, S. J., Hagen, S., & Xu, K. (2023). Land loss due to human-altered sediment budget in the Mississippi River Delta. *Nature Sustainability*, 6(6), 1-8. <http://dx.doi.org/10.1038/s41893-023-01081-0>.
- Estigoni, M. V. (2016). *Uso de modelagem de transporte de sedimentos e técnicas de hidrologia estatística para redução de incertezas nos estudos de assoreamento de reservatórios: estudo de caso do reservatório da PCH Mogi-Guaçu-SP* (Tese de doutorado). Universidade de São Paulo, São Carlos. Retrieved in 2023, December 1, from <https://www.teses.usp.br/teses/disponiveis/18/18139/tde-10022017-085647/en.php>

- Figueiredo, M. D., Lameiras, F. S., Ardisson, J. D., Araujo, M. H., & Teixeira, A. P. de C. (2019). Tailings from Fundao tragedy: physical ~ echemical properties of the material that remains by Candonga dam. *Integrated Environmental Assessment and Management*, 16(5), 636-642. <http://dx.doi.org/10.1002/ieam.4227>.
- Fortugno, D., Boix-Fayos, C., Bombino, G., Denisi, P., Quiñonero Rubio, J. M., Tamburino, V., & Zema, D. A. (2017). Adjustments in channel morphology due to land-use changes and check dam installation in mountain torrents of Calabria (southern Italy). *Earth Surface Processes and Landforms*, 42(14), 2469-2483. <http://dx.doi.org/10.1002/esp.4197>.
- Frachini, E., Ferreira, C. S. R., Kroetz, B. L., Urbano, A., Abrão, T., & Santos, M. J. (2021). Modeling the kinetics of potentially toxic elements desorption in sediment affected by a dam breakdown disaster in Doce River-Brazil. *Chemosphere*, 283, 131157. <http://dx.doi.org/10.1016/j.chemosphere.2021.131157>.
- Fraga, M. D. S., Reis, G. B., da Silva, D. D., Guedes, H. A. S., & Elesbon, A. A. A. (2020). Use of multivariate statistical methods to analyze the monitoring of surface water quality in the Doce River basin, Minas Gerais, Brazil. *Environmental Science and Pollution Research International*, 27(28), 35303-35318. <http://dx.doi.org/10.1007/s11356-020-09783-0>.
- Fundação Renova. (2023). *Monitoramento Rio Doce – PMQQS*. Retrieved in 2023, December 1, from <https://monitoramentoriadoce.org>
- Ghosh, A., Roy, M. B., Roy, P. K., & Mukherjee, S. (2021). Assessing the nature of sediment transport with bridge scour by 1D sediment transport model in the sub-catchment basin of Bhagirathi–Hooghly river. *Modeling Earth Systems and Environment*, 7(4), 2823-2845. <http://dx.doi.org/10.1007/s40808-020-01058-4>.
- Google Earth. (2023). Retrieved in 2023, December 1, from <https://earth.google.com>
- Grzegorzczuk, V., Santos, M. L., & Pagotto, D. (2019). As características sedimentares do transporte da carga de fundo nas confluências do Rio Ivinhema-MS com o Rio Paraná. *RAEGA-O Espaço Geográfico em Análise*, 46(1), 41-57. <http://dx.doi.org/10.5380/raega.v46i1.54140>.
- Gudgeirsdóttir, E. S. (2023). *Assessment of a sediment management solution in a reservoir with a sluicing technique using a HEC-RAS 2D model: Case study of Andakléisá river in west Iceland*. Retrieved in 2023, December 1, from <https://kth.diva-portal.org/smash/record.jsf?pid=diva2%3A1801519&dsid=5096>
- Hagg, W., Ram, S., Klaus, A., Aschauer, S., Babernits, S., Brand, D., Guggemoos, P., & Pappas, T. (2021). Hazard assessment for a glacier lake outburst flood in the Mo Chu River Basin, Bhutan. *Applied Sciences*, 11(20), 9463. <http://dx.doi.org/10.3390/app11209463>.
- Haghiabi, A. H., & Zaredehdasht, E. (2012). Evaluation of HEC-RAS ability in erosion and sediment transport forecasting. *World Applied Sciences Journal*, 17(11), 1490-1497. Retrieved in 2023, December 1, from <https://www.academia.edu/download/44701578/10.1.1.389.6122.pdf>
- Hallinan Junior, A. J. (1993). A review of the Weibull distribution. *Journal of Quality Technology*, 25(2), 85-93. <http://dx.doi.org/10.1080/00224065.1993.11979431>.
- Holly Junior, F. M., & Preissmann, A. (1977). Accurate calculation of transport in two dimensions. *Journal of the Hydraulics Division*, 103(11), 1259-1277. <http://dx.doi.org/10.1061/JYCEAJ.0004870>.
- Instituto Brasileiro de Geografia e Estatística – IBGE. (2016). *IBGE 2016 metadata*. Rio de Janeiro.
- Jesus, J. B., & Nascimento, Y. S. (2020). Tempo de retorno e espacialização das precipitações máximas pelo método dos momentos para o estado da Bahia. *Engenharia Sanitária e Ambiental*, 25(1), 127-131. <http://dx.doi.org/10.1590/s1413-41522020200508>.
- Kroukamp, E., & Wepener, V. (2022). Toxic trace metals in the environment, a study of water pollution. In J. Gailer, & R. J. Turner (Eds.), *Environmental and biochemical toxicology: concepts, case studies and challenges* (pp. 191). Berlin: Walter de Gruyter GmbH. <http://dx.doi.org/10.1515/9783110626285-008>.
- Laurence, D., Franke, C., Alary, C., Delplanque, M., & De Windt, L. (2022). Fingerprinting approach to trace sedimentary and contaminant sources in a canalized section of the Scheldt river (Northern France) for watershed management. In *EGU General Assembly Conference Abstracts* (pp. EGU22-3861). Göttingen: Copernicus Gesellschaft mbH.
- Leite Ribeiro, M., Blanckaert, K., & Schleiss, A. J. (2016). Local tributary widening for river rehabilitation. *Ecobydrology*, 9(2), 204-217. <http://dx.doi.org/10.1002/eco.1588>.
- Leli, I. T., Stevaux, J. C., Bennert, A., Santos, V. C., & Luz, L. D. (2023). Morphological resilience at the confluence of a very low discharge creek and a large river (upper Parana, Brazil). *Journal of South American Earth Sciences*, 123, 104222. <http://dx.doi.org/10.1016/j.jsames.2023.104222>.
- Lima, J. E. F. W., Lopes, W. T. A., Carvalho, N. D. O., Vieira, M. R., & Silva, E. D. (2005). Suspended sediment fluxes in the large river basins of Brazil. In *Sediment Budgets I (Proceedings of the 7th LAHS Scientific Assembly)* (pp. 1-9), Foz do Iguaçu, Brazil. Retrieved in 2023, December 1, from https://www.researchgate.net/profile/Jorge-Enoch-Lima/publication/235968931_Suspended_sediment_fluxes_in_the_large_river_basins_of_Brazil/links/5694dd3708ae3ad8e33cda8c/Suspended-sediment-fluxes-in-the-large-river-basins-of-Brazil.pdf
- Liu, X., Li, L., Hua, Z., Tu, Q., Yang, T., & Zhang, Y. (2019). Flow dynamics and contaminant transport in Y-shaped river channel confluences. *International Journal of Environmental Research and Public Health*, 16(4), 572. <http://dx.doi.org/10.3390/ijerph16040572>.
- Lopes, N. P., Freitas, R. P. D., & Rocha, R. C. (2019). How many more Brumadinhos and Marianas Will We be faced with yet. *Journal of the Brazilian Chemical Society*, 30, 681-682. <http://dx.doi.org/10.21577/0103-5053.20190034>.

- Luz, L. D., Szupiany, R. N., Parolin, M., Silva, A., & Stevaux, J. C. (2020). Obtuse-angle vs. confluent sharp meander bends: insights from the Paraguay-Cuiabá confluence in the tropical Pantanal wetlands, Brazil. *Geomorphology*, *348*, 106907. <http://dx.doi.org/10.1016/j.geomorph.2019.106907>.
- Machado, N. C. (2017). *Retrospectiva da proteção decorrente da ruptura da Barragem do Fundão com diferentes modelos numéricos e hipóteses de simulação* (Dissertação de mestrado). Universidade Federal de Minas Gerais, Belo Horizonte. Retrieved in 2023, December 1, from <https://repositorio.ufmg.br/handle/1843/BUOS-AV3MTA>.
- Magliulo, P., & Valente, A. (2020). GIS-Based geomorphological map of the Calore River floodplain near Benevento (Southern Italy) overflowed by the 15th October 2015 event. *Water*, *12*(1), 148. <http://dx.doi.org/10.3390/w12010148>.
- Magliulo, P., Bozzi, F., Leone, G., Fiorillo, F., Leone, N., Russo, F., & Valente, A. (2021). Channel adjustments over 140 years in response to extreme floods and land-use change, Tammara River, southern Italy. *Geomorphology*, *383*, 107715. <http://dx.doi.org/10.1016/j.geomorph.2021.107715>.
- Marciano, A. G. (2019). *Modelagem Hidrodinâmica com a integração do mapeamento das inundações do rio Sapucaí do município de Itajubá/MG* (Dissertação de mestrado). Universidade Federal de Itajubá, Itajubá. Retrieved in 2023, December 1, from <https://repositorio.unifei.edu.br/jspui/handle/123456789/1968>
- Marx, A. (2023). *Development of a two-dimensional hydraulic model to evaluate sediment deposition after the Klamath dam removal* (Honors college thesis). Oregon State University. Honors College, Oregon. Retrieved in 2023, December 1, from https://ir.library.oregonstate.edu/concern/honors_college_theses/st74d0055
- Miyawaki, S., Constantinescu, G., Rhoads, B., & Sukhodolov, A. (2010). Changes in three-dimensional flow structure at a river confluence with changes in momentum ratio. *River Flow*, *2010*, 225-232. Retrieved in 2023, December 1, from https://izw.baw.de/e-medien/river-flow-2010/PDF/A1/A1_23.pdf
- Mohammed, H. S., Alturfi, U. A., & Shlash, M. A. (2018). Sediment transport capacity in Euphrates river at Al-Abbasia reach using Hec-Ras model. *International Journal of Civil Engineering and Technology*, *9*(5), 919-929. Retrieved in 2023, December 1, from https://www.researchgate.net/profile/Marwah-Shlash/publication/328497503_Sediment_Transport_Capacity_IN_Euphrates_RIVER_AT_AL-ABBASIA_REACH_using_HEC-RAS_model/links/5e9d96a94585150839ec3b97/Sediment-Transport-Capacity-IN-Euphrates-RIVER-AT-AL-ABBASIA-REACH-using-HEC-RAS-model.pdf
- Mosher, S. J., & Martini, I. P. (2002). Coarse-grained flood bars formed at the confluence of two subarctic rivers affected by hydroelectric Dams, Ontario, Canada. In P. Martini, V. R. Baker, & G. Garzón (Eds.), *Flood and megaflood processes and deposits: recent and ancient examples* (pp. 211-231). Chichester: Wiley. <http://dx.doi.org/10.1002/9781444304299.ch12>.
- Mosley, M. P. (1976). An experimental study of channel confluences. *The Journal of Geology*, *84*(5), 535-562. <http://dx.doi.org/10.1086/628230>.
- Mosley, M. P. (1979). Streamflow generation in a forested watershed, New Zealand. *Water Resources Research*, *15*(4), 795-806. <http://dx.doi.org/10.1029/WR015i004p00795>.
- Mourão, A. O., Santos, M. S., da Costa, A. S. V., da Silva, H. T., Maia, L. F. O., Faria, M. C. D. S., Rodriguez, M. V. R., & Rodrigues, J. L. (2023). Assessment of health risk and presence of metals in water and fish samples from doce river, Brazil, after fundão dam collapse. *Archives of Environmental Contamination and Toxicology*, *84*(3), 1-12. <http://dx.doi.org/10.1007/s00244-023-00991-6>.
- Nazari-Giglou, A., Jabbari-Sahebari, A., Shakibaenia, A., & Borghei, S. M. (2016). An experimental study of sediment transport in channel confluences. *International Journal of Sediment Research*, *31*(1), 87-96. <http://dx.doi.org/10.1016/j.ijsrc.2014.08.001>.
- Nelson, C. E., Wegley Kelly, L., & Haas, A. F. (2023). Microbial interactions with dissolved organic matter are central to coral reef ecosystem function and resilience. *Annual Review of Marine Science*, *15*(1), 431-460. <http://dx.doi.org/10.1146/annurev-marine-042121-080917>.
- Oliveira, B. L. F. D., Davis, E. G., Matos, A. J. S., & Coelho Filho, J. A. P. (2022). *Operação do sistema de alerta hidrológico da bacia do rio Doce 2022*. Belo Horizonte: CPRM. Retrieved in 2023, December 1, from https://rigeo.cprm.gov.br/bitstream/doc/23174/1/Operacao%20Sistema%20de%20Alerta_Rio%20Doce_2022.pdf
- Pakam, S., Ahmed, A., Ebraheem, A. A., Sherif, M., Mirza, S. B., Ridouane, F. L., & Sefelnasr, A. (2023). Risk Assessment and mapping of flash flood vulnerable zones in Arid Region, Fujairah City, UAE-using remote sensing and GIS-based analysis. *Water*, *15*(15), 2802. <http://dx.doi.org/10.3390/w15152802>.
- Palu, M. C. (2019). *Floodwave and sediment transport assessment along the Doce river after the Fundão tailings dam collapse (Brazil)* (Tese de doutorado). Colorado State University, Colorado. Retrieved in 2023, December 1, from <https://search.proquest.com/openview/w/5cc1e9d1181398464eaa52e56b3b8db4/1?pq-origsite=gscholar&cbl=18750&diss=y>.
- Paulelli, A. C. C., Cesila, C. A., Devóz, P. P., de Oliveira, S. R., Ximenez, J. P. B., dos Reis Pedreira Filho, W., & Barbosa Jr, F. (2022). Fundão tailings dam failure in Brazil: evidence of a population exposed to high levels of Al, As, Hg, and Ni after a human biomonitoring study. *Environmental Research*, *205*, 112524. <http://dx.doi.org/10.1016/j.envres.2021.112524>.
- Rangel, B. D. A. (2021). *Comportamento morfológico no delta do rio Magdalena (Colômbia) devido as variações da vazão em escala intra e interanual* (Tese de doutorado). Universidade Federal do Rio de Janeiro, Rio de Janeiro. Retrieved in 2023, December 1, from https://w1.files.solucaoatrio.net.br/atrio/ufrj-peno_upl/THESIS/10002785/doutorado_borisavila_20220304081600403.pdf.

- Rhoads, B. L. (2006). The dynamic basis of geomorphology reenvisioned. *Annals of the Association of American Geographers*, 96(1), 14-30. <http://dx.doi.org/10.1111/j.1467-8306.2006.00496.x>.
- Rhoads, B. L. (2020). *River dynamics: geomorphology to support management*. Cambridge: Cambridge University Press. <http://dx.doi.org/10.1017/9781108164108>
- Rhoads, B. L., & Kenworthy, S. T. (1995). Flow structure at an asymmetrical stream confluence. *Geomorphology*, 11(4), 273-293. [http://dx.doi.org/10.1016/0169-555X\(94\)00069-4](http://dx.doi.org/10.1016/0169-555X(94)00069-4).
- Rice, S. P., Kiffney, P., Greene, C., & Pess, G. R. (2008). The ecological importance of tributaries and confluences. In S. P. Rice, A. G. Roy, & B. L. Rhoads (Eds.), *River confluences, tributaries and the fluvial network* (pp. 209-242). Hoboken: Wiley. <http://dx.doi.org/10.1002/9780470760383.ch11>.
- Righini, M., Surian, N., Wohl, E., Marchi, L., Comiti, F., Amponsah, W., & Borga, M. (2017). Geomorphic response to an extreme flood in two Mediterranean rivers (northeastern Sardinia, Italy): analysis of controlling factors. *Geomorphology*, 290, 184-199. <http://dx.doi.org/10.1016/j.geomorph.2017.04.014>.
- Rosa, D. W. B. (2017). *Resposta hidrológica de uma bacia hidrográfica urbana à implantação de técnicas compensatórias de drenagem urbana-Bacia do Córrego do Leitão* (Dissertação de mestrado). Universidade Federal de Minas Gerais, Belo Horizonte. Retrieved in 2023, December 1, from <http://hdl.handle.net/1843/BUBD-AUEEXV>.
- Roy, A. G., Roy, R., & Bergeron, N. (1988). Hydraulic geometry and changes in flow velocity at a river confluence with coarse bed material. *Earth Surface Processes and Landforms*, 13(7), 583-598. <http://dx.doi.org/10.1002/esp.3290130704>.
- Samson, R., Shah, M., Yadav, R., Sarode, P., Rajput, V., Dastager, S. G., Dharné, M. S., & Khairnar, K. (2019). Metagenomic insights to understand transient influence of Yamuna River on taxonomic and functional aspects of bacterial and archaeal communities of River Ganges. *The Science of the Total Environment*, 674, 288-299. <http://dx.doi.org/10.1016/j.scitotenv.2019.04.166>.
- Sanchis-Ibor, C., Segura-Beltrán, F., & Navarro-Gómez, A. (2018). Channel forms and vegetation adjustment to damming in a Mediterranean gravel-bed river (Serpis River, Spain). *River Research and Applications*, 35(1), 37-47. <http://dx.doi.org/10.1002/rra.3381>.
- Santos, G. O. S., Rodrigues, J. V., Barbosa, L. A., da Silva Batista, L., & Pereira, R. G. (2021). Considerações sobre enchentes e inundações em Governador Valadares. *Jornada Acadêmica das Engenharias*, 2(1), 1. Retrieved in 2023, December 1, from <https://periodicos.univale.br/index.php/jae/article/view/86/79>
- Santos, V. C., & Stevaux, J. C. (2017). Fluvial processes and morphology in river channel confluences: a review. *Revista Brasileira de Geomorfologia*, 18(1), 3-17.
- Shaikh, A. A., Pathan, A. I., Waikhom, S. I., Agnihotri, P. G., Islam, M. N., & Singh, S. K. (2023). Application of latest HEC-RAS version 6 for 2D hydrodynamic modeling through GIS framework: a case study from coastal urban floodplain in India. *Modeling Earth Systems and Environment*, 9(1), 1369-1385. <http://dx.doi.org/10.1007/s40808-022-01567-4>.
- Shelley, J. E. (2021). *Modeling the effect of increased sediment loading on bed elevations of the Lower Missouri River*. Washington, DC: ERDC Knowledge Core. <http://dx.doi.org/10.21079/11681/40360>.
- Shrestha, S., Imbulana, N., Piman, T., Chonwattana, S., Ninsawat, S., & Babur, M. (2020). Multimodelling approach to the assessment of climate change impacts on hydrology and river morphology in the Chindwin River Basin, Myanmar. *Catena*, 188, 104464. <http://dx.doi.org/10.1016/j.catena.2020.104464>.
- Shukla, P. K., Singha, D. K., & Sain, K. (2022a). Modeling of in-situ horizontal stresses and orientation of maximum horizontal stress in the gas hydrate-bearing sediments of the Mahanadi offshore basin, India. *Geomechanics and Geophysics for Geo-Energy and Geo-Resources*, 8(3), 90. <http://dx.doi.org/10.1007/s40948-022-00401-6>.
- Shukla, T., Lewis, Q. W., & Rhoads, B. L. (2022b). Spatial patterns of transport-effective flow at three small confluences: relation to channel morphology. *Earth Surface Processes and Landforms*, 48(5), 1011-1033. <http://dx.doi.org/10.1002/esp.5532>.
- Sposito, E. C. (2021). *Uso e cobertura do solo na bacia hidrográfica do rio Doce (MG/ES): inter-relações para a governança* (Tese de doutorado). Universidade Federal de Viçosa, Viçosa. Retrieved in 2023, December 1, from <https://locus.ufv.br/handle/123456789/29478>.
- Stevaux, J. C., Amâncio, A., Carlos Etchebehere, M. L., & Fujita, R. H. (2009). Flow structure and dynamics in large tropical River confluence: example of the Ivaí and Paraná Rivers, southern Brazil. *Geociências*, 28(2), 5-13. Retrieved in 2023, December 1, from <https://biblat.unam.mx/hevila/GeocienciasSaoPaulo/2009/vol28/no1/1.pdf>
- Sukhodolov, A. N., Shumilova, O. O., Constantinescu, G. S., Lewis, Q. W., & Rhoads, B. L. (2023). Mixing dynamics at river confluences governed by intermodal behaviour. *Nature Geoscience*, 16(1), 89-93. <http://dx.doi.org/10.1038/s41561-022-01091-1>.
- Thomson, K. D., Stockli, D. F., & Fildani, A. (2022). Anthropogenic impact on sediment transfer in the upper Missouri River catchment detected by detrital zircon analysis. *Geological Society of America Bulletin*, 134(9-10), 2485-2502. <http://dx.doi.org/10.1130/B36217.1>.
- Turra, T. M., Marques, V. V., & Stevaux, J. C. (1999). Confluence bar of the São Pedro Brook in the Paraná River: genesis and environmental importance. *Boletim Goiano de Geografia*, 19(1), 8. Retrieved in 2023, December 1, from <https://dialnet.unirioja.es/descarga/articulo/4785560.pdf>

Wu, W. (2004). Depth-averaged two-dimensional numerical modeling of unsteady flow and nonuniform sediment transport in open channels. *Journal of Hydraulic Engineering*, 130(10), 1013-1024. [http://dx.doi.org/10.1061/\(ASCE\)0733-9429\(2004\)130:10\(1013\)](http://dx.doi.org/10.1061/(ASCE)0733-9429(2004)130:10(1013)).

Wu, W., & Wang, S. S. (2006). Formulas for sediment porosity and settling velocity. *Journal of Hydraulic Engineering*, 132(8), 858-862. [http://dx.doi.org/10.1061/\(ASCE\)0733-9429\(2006\)132:8\(858\)](http://dx.doi.org/10.1061/(ASCE)0733-9429(2006)132:8(858)).

Yan, X., Jiao, J., Li, M., Qi, H., Liang, Y., Xu, Q., Zhang, Z., Jiang, X., Li, J., Zhang, Z., & Wang, H. (2022). Lateral sediment connectivity of landslides occurred under a heavy rainstorm and its influence on sediment yield of slope-channel cascade on the loess plateau. *Catena*, 216, 106378. <http://dx.doi.org/10.1016/j.catena.2022.106378>.

Yu, Q., Yuan, S., & Rennie, C. D. (2020). Experiments on the morphodynamics of open channel confluences: implications for the accumulation of contaminated sediments. *Journal of Geophysical Research: Earth Surface*, 125(9), e2019JF005438. <http://dx.doi.org/10.1029/2019JF005438>.

Yuan, S. Y., Xu, L., Tang, H. W., Xiao, Y., & Gualtieri, C. (2022). A dinâmica das confluências fluviais e seus efeitos na ecologia do ambiente aquático: uma revisão. *Journal of Hydrodynamics*, 34(1), 1-14. <http://dx.doi.org/10.1007/s42241-022-0001-z>.

Yuan, S., Tang, H., Li, K., Xu, L., Xiao, Y., Gualtieri, C., Rennie, C., & Melville, B. (2021). Hydrodynamics, sediment transport and morphological features at the confluence between the Yangtze River and the Poyang Lake. *Water Resources Research*, 57(3), e2020WR028284. <http://dx.doi.org/10.1029/2020WR028284>.

Zawiejska, J., Wyżga, B., & Radecki-Pawlik, A. (2015). Variation in surface bed material along a mountain river modified by gravel extraction and channelization, the Czarny Dunajec, Polish Carpathians. *Geomorphology*, 231, 353-366. <http://dx.doi.org/10.1016/j.geomorph.2014.12.026>.

Authors contributions

Alexandre Germano Marciano: Main author of the article, generation of most of the results, field data collection, data analysis and writing of the article.

Arcilan Trevenzoli Assireu: Research supervisor, field data collection, analysis of results and review of the text.

Samara Calçado de Azevedo: Manipulation of topography data and text review.

Benedito Cláudio da Silva: Simulation data manipulation and text review.

Adriana Tropia de Abreu: Particle size data manipulation and text review

Hermínio Arias Nalini Júnior: Discussion of results and text review.

Editor-in-Chief: Adilson Pinheiro

Associated Editor: Iran Eduardo Lima Neto